Optimization of the *in vitro* Canine Oviduct Epithelium Culture System

R. Carranza Villarejo (Rocío)

Supervisors: dr. H.H.W. Henning,
dr. J. de Gier
Utrecht University, Faculty of Veterinary Medicine,
Graduate School of Life Sciences
December 28, 2022

Abstract

To date, most assisted reproductive technologies in canid species remain poorly successful. This may be attributed to physiological differences in the bitch; mainly, the meiotic resumption of the oocyte in the oviduct, after being released in germinal vesicle stage from the ovary. This represents a major challenge for harvesting mature oocytes; thus, in vitro maturation (IVM) of canine oocytes is required. Recent studies have shown that co-culturing immature oocytes with oviduct epithelial cells (cOEC) increases the chances of oocyte meiotic resumption in vitro. However, the current protocols for isolating and culturing cOECs have failed to provide a favorable environment for IVM. In the present study we aimed to optimize the isolation of cOEC and culturing a monolayer system with Transwell® inserts. We hypothesized that the introduction of an air-liquid interface, in combination with the inhibition of the Notch pathway, would stir cOEC differentiation towards a morphology that more closely resembles the in vivo oviduct epithelium. We successfully managed to isolate cOECs from 15 bitches by enzymatic digestion and mechanic squeezing of the ex vivo oviducts obtained by elective ovariectomy in anestrus. Cells were directly seeded in Transwell inserts and cultured, first, for 7 days in a liquid-liquid interface, which allowed them to de-differentiate and form a confluent monolayer; then, 16 days in an air-liquid interface where they polarized into a columnar shape and re-differentiated into ciliated and non-ciliated cells. After, 10 more days of culturing in an air-liquid interface with the addition of DBZ, to further stimulate ciliation. Confluence of the monolayers was assessed by measuring the transepithelial electrical resistance.

By immunofluorescent staining, we found two main morphological categories of monolayers, low and high cell-density monolayers. The former, characterized by the presence of flat, irregular-shaped, unpolarized cells. The latter, resembling the desired morphology the most, with polarized columnar cells; nevertheless, the presence of ciliated cells after introducing the air-liquid interface, remained below 20%.

Treatment with DBZ only enhanced ciliation significantly in monolayers containing >15% ciliated cells, preceding the treatment. To determine the effects of DBZ on ciliogenesis related transcription factors FOXJ1 and RFX1, and Notch primary target genes, we performed qRT-PCR assays on two high cell-density monolayer samples. Expression fold change profiles were mostly consistent with our theoretical hypothesis: upregulation in transcription factors FOXJ1 and RFX1 and a downregulation in target genes HES1 and HEY1.

Overall, high cell-density monolayers resembled the *in vivo* morphology the most. However, functionality and long-term sustainability of the model remain unknown. This study provides a good foundation for further optimization of the cOEC monolayer Transwell® model.

Summary Sentence

Canine oviduct epithelial cells were isolated and cultured in Transwell® inserts to promote the formation and differentiation of confluent monolayers that resemble the *in vivo* oviduct lining morphology.

Layman's Summary

Currently, the standard methods of assisted reproduction, such as *in vitro* fertilization, remain poorly successful in canine species. Past studies have shown that by mimicking the natural environment where fertilization occurs in the dog, known as the oviduct, the chances of success increase significantly. Therefore, our aim in this study was to create a model that closely resembles this environment. To do this, we extracted cells from the inside of the dog oviduct, seeded them in porous membranes called Transwell® inserts and cultured them for 33 days. We divided the inserts into two sample groups: a control group, where the conditions remained constant for the culturing period; and a treated group, where, for the last ten days of culture, we supplemented the cells with a molecule called DBZ, which is believed to help achieve the desired morphology.

In both the control and treated sample groups we found two types of morphologies: one we called "low cell-density" which was characterized by very few, big, flat cells, and another called "high cell-density", with hundreds of small, columnar-shaped cells, which more closely resemble the natural morphology the most.

We found that treating the cells with DBZ only had a significant effect on the high cell-density samples and it indeed helped those cells achieve a closer resemblance to the natural environment of the dog oviduct. These results are a good starting point for the oviduct model; however, we are yet to test if this model is functional for canine assisted reproduction.

Key words: canine oviduct epithelial cells, secondary cilia, Notch pathway, cell differentiation, Transwell inserts.

Introduction

Assisted reproductive technologies (ART) in canid species remain a highly relevant field of research due to their multiple applications, such as understanding human genetic mechanisms of disease by using the dog as a biomedical model, the improvement of animal health and welfare by enabling removal of deleterious genetic traits in specific breeds, conservation of rare or endangered breeds and translation to other canid species such as the fox or wolf; and finally, for commercial breeding purposes.

The female canine reproductive physiology is characterized by a nonseasonal, monoestrous cycle, with a lengthy anestrus phase that ranges from 4 to 10 months and a follicular phase where an oocyte in germinal vesicle stage is released from the ovary. The oocyte performs meiotic resumption in the oviduct until it reaches metaphase II stage, around 2-3 days after ovulation, and possesses a high lipid content, which gives a dark appearance to the cytoplasm. (Hu, et al. 2020; Albers-Wolthers, 2017) These unique physiological and morphological traits have represented major challenges for the success of canine *in vitro* ARTs such as in vitro oocyte maturation (IVM) and *in vitro* fertilization (IVF) systems, with rates of <30% oocytes reaching metaphase stages and <10%, typical fertilization. (Chastant-Maillard, et al. 2012; No, et al. 2018)

A plausible explanation for these low IVM and IVF rates could be attributed to the limited developmental capacity of oocytes harvested at anestrus, due to the lower risk of complications during gonadectomy. However, recent reports have shown that canine oocytes cocultured with oviduct epithelial cells present a higher meiotic resumption competence, but the development potential of these oocytes remains to be evaluated. (No, et al. 2018).

In vitro oviduct models

The oviduct is the anatomical region that connects the ovary to the uterus and consists of three parts: the infundibulum, the ampulla and isthmus. The infundibulum is the ovarian end of the oviduct and its main function is to surround the ovary to capture the newly ovulated oocyte and transport it to the following section of the oviduct: the ampulla. The ampulla serves as a meiosis resumption and fertilization site for the canine oocyte. Through epithelial cell beating cilia and smooth muscle contractions, the ampulla holds the oocyte until the final maturation stage, allows fertilization to take place and, finally, transports it to the uterine end of the oviduct: the isthmus, which leads the gamete or embryo into the uterus, by the utero-tubal junction. (Senger, et al. 2012; Coy, et al. 2012)

The oviducts inner layer, called mucosa, is composed of epithelium folds that consist mainly of simple cuboidal to columnar cells, with heterogeneous distribution of both ciliated and secretory cells. (Senger, et al. 2012; Ferraz, et al. 2016; Coy, et al. 2012) The ratio of ciliated to secretory cells vary among the estrus stage and the oviductal region, with the highest number of ciliated cells during late follicular and mid-luteal phase in the infundibulum (>60%) and the lowest, during anestrus in the isthmus area (<1%). (Steinhauer, et al. 2004)

The idea of establishing an *in vitro* oviduct model raises the possibility of mimicking, and studying, the *in vivo* oviduct epithelial cell environment regarding protein expression, ciliary and secretory activity, and responses to physiological stimuli. Harvesting methods for oviduct epithelial cells (OECs) in diverse species, including canids, are most performed *ex vivo*, and methods to culture OECs are variable with respect to cell isolation techniques, culture conditions, duration, medium used and growth supplements. (Ferraz, et al. 2016, Ulbrich, et al. 2010)

Previous studies in multiple mammalian species have shown that when oviduct epithelial cells are simply plated and grown in a petri dish, forming a 2-D culture, they quickly dedifferentiate into flattened cells and almost completely lose their cilia or secretory activity, within other functions. (Sostaric, et al. 2008) The loss-of-function and loss-of-morphology have been improved by the introduction of cell inserts with separate compartments, such as the Transwell® inserts, that allow a better cell polarization and differentiation in an air-liquid interface, for a long-term culture with a mixed population of secretory and ciliated cells (Fig.1) (Chen, et al. 2013; Gualtieri, et al. 2013). A recent report has shown that a canine oviduct Transwell®-based model allowed for cell polarization and differentiation; however, the proportion of ciliated cells present in the culture was significantly lower than cells with no secondary cilia, and the culture was not responsive to hormonal (progesterone, estradiol, FSH and LH) stimuli. (Meeuws, 2019) The main aim of this study is to establish an optimized Transwell®-based cell culture system of cOEC with a balanced presence of ciliated and non-ciliated cells, to create an *in vitro* oviduct model that provides a favorable environment for IVM and IVF.

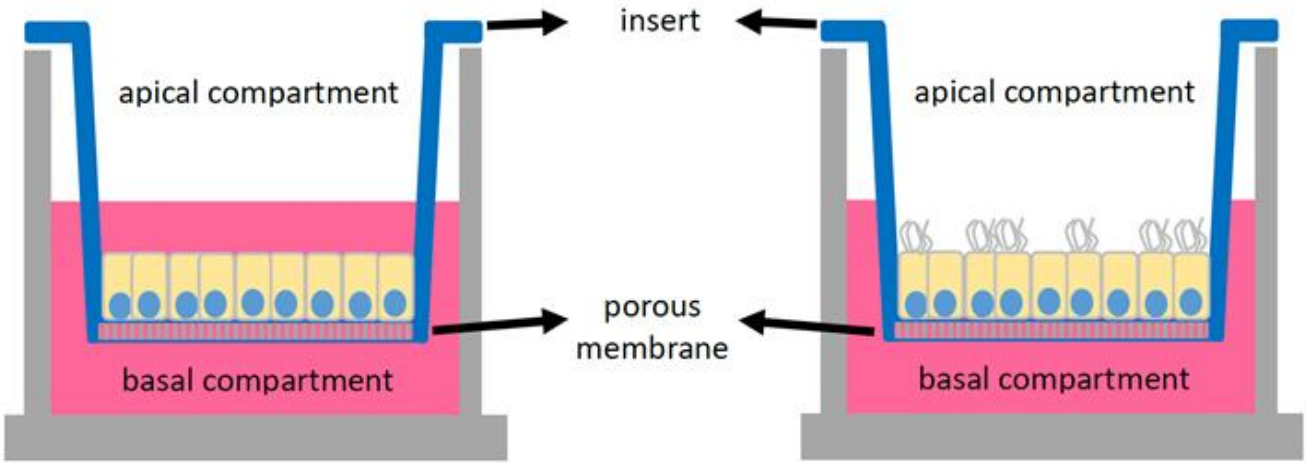

Fig 1. Transwell® insert compartmentalized cell culture principle.

Other, more complex, culture systems proven to promote cell polarization and differentiation are the 3-D culture systems, such as organoids and organs-on-a-chip. Organoids are self-organizing structures with robust constant growth and self-renewal that have shown to mimic the native tissue architecture, such as mucosal folds for oviduct models. (Kessler, et al. 2015) The organ-on-a-chip approach to creating *in vitro* models (oviduct-on-a-chip) is based on the highly sophisticated microfluidic engineering of different levels of cell organization and dynamic interaction, allowing flow, perfusion, and a more controlled compartmentalization for a faithful recapitulation of native tissue architecture. More recently, it has been shown in a canine oviduct-on-a-chip system that efficient genetic engineering tools, such as CRISP-Cas9, can have a high efficiency rate. (Ferraz, et al. 2020)

For this study, the simplicity of a canine oviduct epithelial cell Transwell® model is ideal, because it allows a sufficient visualization of cell polarization and differentiation to analyze and determine the ciliated to non-ciliated cell ratio present in a monolayer.

The Notch pathway and its role in epithelial cell fate and ciliogenesis

Since the Transwell®-based canine oviduct model has not been responsive to hormone changes, as previously mentioned, other approaches to stir ciliated cell differentiation are necessary. The Notch signaling pathway is a highly conserved mechanism that has a central role in deciding the fate of a variety of developmental processes, including ciliogenesis, in many cell types. (Choksi, et al. 2014; Sparrow, et al. 2002; Andersson, et al. 2011) When associated with epithelial cells, more specifically the airway and oviductal models in multiple mammal species such as human, mouse, swine, among others, the Notch pathway has been proven to regulate the equilibrium of ciliated and secretory cells. (Kessler, et al. 2015; Murta, et al. 2015; Tsao, et al. 2009; Zhu, et al. 2019) However,

the molecular mechanisms behind this balance are not yet fully understood and whether these findings are translational to canid species remains to be further studied.

In mammals, four Notch receptors (Notch1-4) and five ligands (delta-like 1 (Dl1) Dl3, Dl4 and Jagged1-2) have been identified. Notch signaling is activated by binding of the extracellular domain of receptors in one cell with ligands expressed in the neighboring cells, which leads to cleavage of the Notch intracellular domain (NICD) by a γ-secretase, followed by its translocation to the nucleus where it triggers the transcriptional regulation of Notch effector genes, such as the hairy/enhancer of split (HESR) genes, which have been identified in female reproductive tissues of humans and mice. (Murta, et al. 2016) Some studies have shown that the Notch pathway promotes differentiation of secretory cells, suggestion that inhibition should trigger differentiation into ciliated cells.

With respect to the cilium, transcription factors RFX1 and RFX2, indirectly inhibited by the Notch pathway, have recently been found to control the transcription of ALMS1, a gene that encodes a basal body-associated protein and that is mutated in the ciliopathy Alström syndrome (Purvis et al. 2010). Moreover, the fact that inactivation of any single RFX factor translates to a rather 'mild' ciliary phenotype further supports a model of functional redundancy and cooperativity among the different RFX factors. Multiple loss-of-function phenotypes in various model organisms, such as zebrafish and mouse embryos and cultured human airway cells, demonstrate that RFX factors appear to be required for the formation of both motile and immotile cilia. (Choksi, et al. 2014).

Another relevant transcription factor with a potential primary role in the regulation and generation of motile cilia is the Forkhead FOXJ1, which has been observed to be expressed in multiple tissues, including the oviductal epithelium. Studies have shown that mice with a loss of FOXJ1 activity lack motile cilia in several tissues (Choksi, et al. 2014; Yu, et al. 2008; Okada, et al. 2004) There is extensive evidence in different model organisms that backup cooperativity between FOXJ1 and RFX transcription factors as shown in Fig 2, however, the clear details of this interaction in canid species remain to be uncovered.

We hypothesize that inhibition of the Notch pathway, by the addition of the γ-secretase inhibitor DBZ, can trigger differentiation into ciliated cells (Kessler, 2015), thus increasing the proportion of ciliated to non-ciliated cells present in the canine oviduct Transwell-culture system. Based on the model provided in Fig. 2, a DBZ treatment of the epithelial cell monolayer should indicate upregulation in the transcription factors FOXJ1 and RFX and downregulation of the NOTCH primary target gene family, HES and HEY.

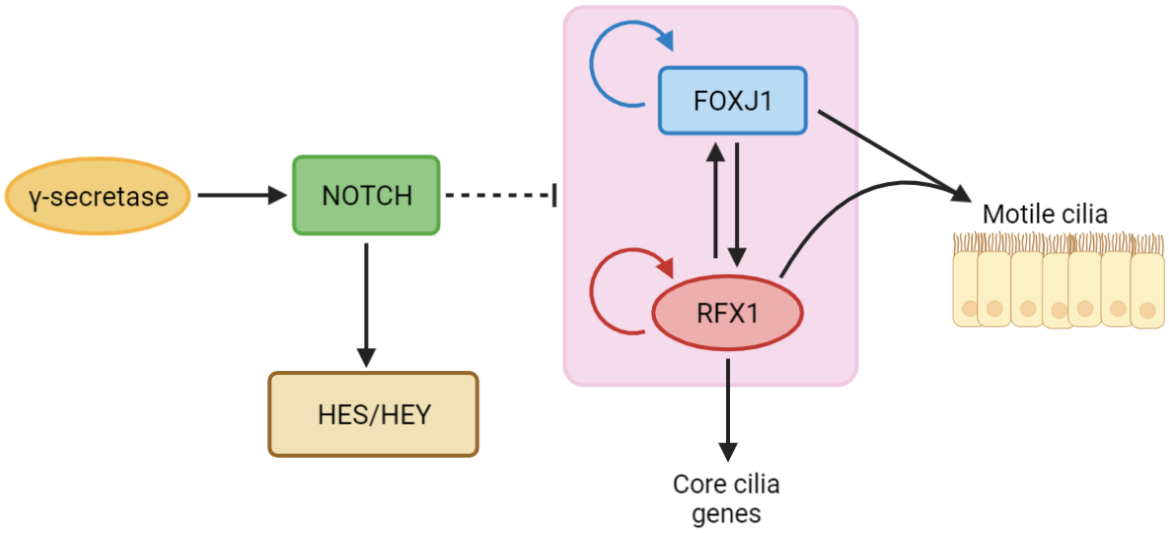

Fig 2. Notch pathway and its role in epithelial cell ciliogenesis. Adapted from Choksi, 2014 and created in BioRender.

Methods

Tissue collection

After elective ovariectomy, either by laparoscopy or laparotomy, pairs of ovarian bursas from 31 privately owned bitches were collected in tubes with either 25 mL phosphate-buffered saline solution supplemented with 100 IU/mL penicillin, 100 µg/mL streptomycin and 50 µg/mL gentamycin (PBS_{PSG}), or tubes with 25 mL of RNA*later* stabilization solution (Invitrogen). Samples collected in PBS_{PSG} were transported on ice, and processed within 30 minutes after ovariectomy. Samples collected in RNA*later* were transported and preserved at room temperature until tissue processing. The research was in line with the animal experimentation guidelines of the Ethical Committee at Utrecht University. All owners were required to sign an informed consent form and supply the following information about the bitch: weight, age, breed and date of last heat.

Oviduct dissection and Canine Oviduct Epithelial Cell (COEC) isolation

A paraffin covered petri dish was mounted on an ice box and each ovarian bursa was fixed with one or two 26G needles (Sterican, B Braun) in the center of the dish, with about 2ml of PBS. The oviduct was dissected from surrounding fat tissue, straightened as much as possible and measured in length. Finally, one quick wash in ethanol followed by three washes in PBS_{PSG} and kept in PBS_{PSG} at ice cold temperature until processing. Oviduct fragments below 2cm of length were discarded.

After removing and discarding the infundibulum and utero-tubal junction, as shown in fig. 3, oviducts were flushed with 3 ml of pre-warmed PBS_{PSG}, filled with 0.5% Trypsin - 0.2% EDTA solution (Sigma-Aldrich), ligated at both ends and incubated for 13 minutes at 37°C in PBS. Then, oviducts were gradually flushed with 3 ml of pre-warmed M199 (Gibco) supplemented with 20% Fetal Bovine Serum (F7524, Sigma-Aldrich), 100 IU/mL penicillin, 100 µg/mL streptomycin and 50 µg/mL gentamicin; henceforth M199*. Mechanic squeezing of the oviducts was performed every 500 µL of M199*.

The isolated cells were collected in a 15 mL tube and centrifuged for 5 min at 50 *g*. The supernatant was removed by vacuum suction and the cell pellet was resuspended in 500 µL of Dulbecco's Modified Eagle Medium/ Nutrient Mixture F-12 (DMEM/F-12) (11320-074, Gibco) supplemented with 10% FBS, 10 ng/mL Epidermal Growth Factor (EGF; E4127, Sigma Aldrich), 5 µg/mL insulin from bovine pancreas (I0516, Sigma Aldrich), 5 µg/mL apo-transferrin (T1428, Sigma Aldrich), 100 IU/mL penicillin, 100 µg/mL streptomycin, 50 µg/mL gentamycin and 1 µg/mL amphotericin B (A2942, Sigma Aldrich), henceforth DMEM/F-12*. Cells were incubated at 37°C (5% CO_2) until further processing.

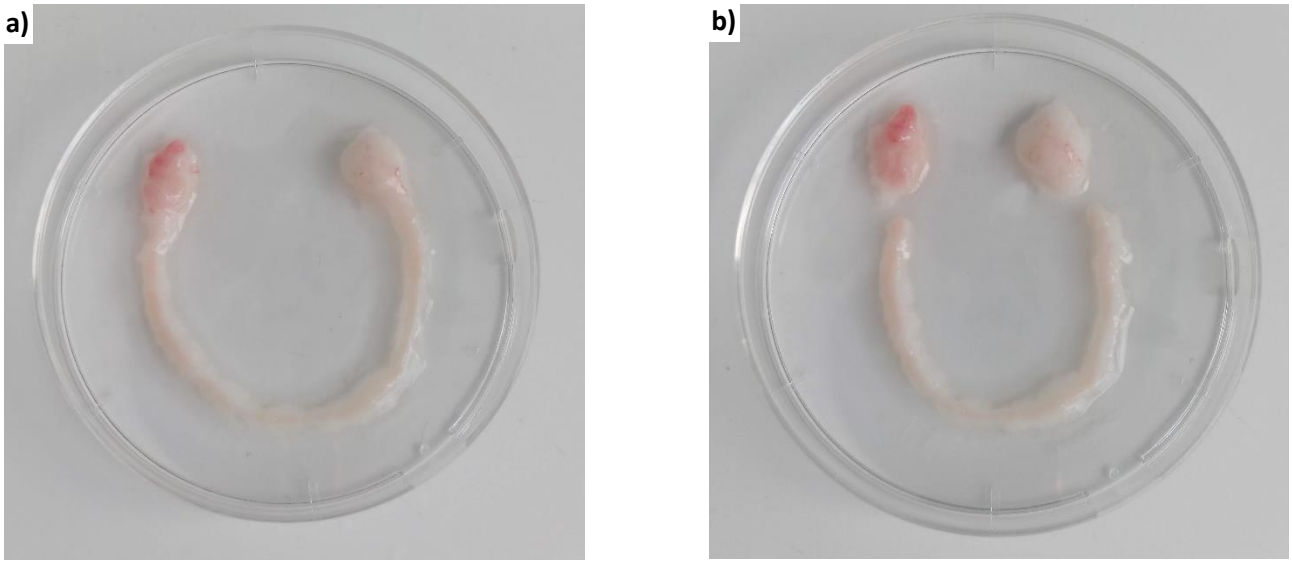

Fig. 3 Canine oviduct dissection. a) Oviducts were dissected from surrounding fat tissue as much as possible. b) The infundibulum (reddish; left-end) and utero-tubal junction (right-end) were removed from the oviduct, prior to flushing.

Cell count and cell viability assessment

30 µL of the resuspended cells were incubated for 5 min with 0.6 µL Hoechst 33342 (stock: 5 mg/mL. Live cells: blue stain) and 0.6 µL propidium iodide (stock: 1 mg/mL. Dead cells: red stain). Estimation of cell concentration was performed with a hemocytometer chamber and a phase contrast microscope (Olympus, CX31). At least 108 squares were counted, containing both isolated and clustered cells.

To determine a representative proportion of viable cells, a minimum of 250 isolated cells (up to four cells clustered together were still considered isolated) and 250 clustered cells, for a total minimum of 500 assessed cells were evaluated with a fluorescence microscope (BH2-RFCA, Olympus) with UV lamp (Olympus, 826506).

Monolayer culture and DBZ treatment

Transwell® insert membranes (6.5 mm diameter, 0.4 µm pore size, polycarbonate membrane, 3413, Costar) were coated with 80 µL of 2% Matrigel (Corning. Lot. 4146004) a day prior to cOEC isolation to improve cell attachment and confluence. (Thomas, et al. 1995)

At least 200,000 viable cells were seeded in the apical compartment of the previously coated Transwell® inserts. The total number of inserts was determined by the viable cell availability and the number of conditions to be tested in each experiment. The inserts were incubated at 37°C with 5% CO_2.

The culturing period lasted 33 days and was divided in three phases: *1. Monolayer-formation phase*; 7 days of liquid-liquid interface (DMEM/F-12*; 200 µL apical compartment, 800 µL basal compartment). Medium was exchanged on day 3 and day 6. *2. Air-liquid interface*; 16 days of air-liquid interface (DMEM/F-12*; 800 µL basal compartment only). Medium was exchanged once a day during weekdays. This phase allowed the cOEC monolayers to become fully confluent, begin polarization and cell-differentiation. *3. DBZ treatment phase*; 10 days of air-liquid interface (DMEM/F-12* supplemented with DBZ 1 or 10 µM; 800 µL basal compartment only) half of the total Transwell® inserts in each experiment were randomly selected for DBZ treatment and other half were supplemented with DMSO as negative controls. This phase allowed cells to fully polarize and differentiate.

The monolayers were assessed for contamination, cluster formation and presence of motile secondary cilia throughout the air-liquid interface and DBZ treatment culture phases, two to three times a week by inverted phase contrast microscopy (Olympus) at 20x magnification.

The monolayers were fixed on day 34 with 4% PFA (200 µL apical compartment, 800 µL basal compartment) and stored at 4°C (for up to two weeks) until further processing.

Transepithelial electrical resistance (TEER) measurement

To assess permeability and integrity of the cOEC monolayers, transepithelial electrical resistance was measured with a Millicell® ERS-2 Volt-ohmmeter (MERS00002, Merck) on day 21 (prior to DBZ treatment, henceforth initial TEER measurement) and day 32 of culturing (post DBZ treatment, henceforth final TEER measurement). Calibration of the device was carried out according to the manufacturer. The electrode was submerged in 70% ethanol for 15 minutes at room temperature, air-dried and rinsed with pre-warmed M199 (37°C). The cOEC monolayer medium was replaced with pre-warmed M199 (37°C; 200 µL apical compartment, 800 µL basal compartment). The inserts were kept on a heated plate at 37°C for the duration of the measurements. Two cell-free Matrigel coated Transwell® inserts, with M199 (200 µL apical compartment, 800 µL basal compartment) were used as blank. Each measurement was performed twice; the electrode was rinsed in pre-warmed M199 after each measurement.

The average resistance for the blank inserts was calculated and subtracted from the average sample resistance. To obtain the true Unit Area Resistance (TEER value), the corrected resistance was multiplied by the membrane area of the Transwell® inserts (0.3 cm^2, according to the manufacturer's user guide).

Immunofluorescence staining

Following fixation with 4% PFA, the cOEC monolayers were washed twice in PBS for 5 minutes and blocked with 5% normal goat serum (Genway 11-511-248003) in PBS including Tween 0.5% (PBST) for 30 minutes. After blocking, three washes with PBST, five minutes each, preceded overnight incubation at 4°C with the primary

antibody: Anti-Acetylated α-Tubulin raised in mouse, as a cilia marker. Dilution of the primary antibody was 1:100 (v:v) in PBST, apical compartment only. Negative control for staining did not include incubation with primary antibody.

Subsequently, cOEC monolayers were washed three times in PBST for five minutes and incubated for two hours at room temperature with the secondary antibody: Goat anti-Mouse Alexa Fluor® 488 (A11029, Invitrogen, Carlsbad, CA, USA). Dilution of secondary antibody was 1:100 (v:v) in PBST, apical compartment only.

Three more PBST washes for five minutes anteceded incubation, for 60 minutes at room temperature, with Hoechst 33342 (1:200; 5 mg/ml) for DNA (nuclei) visualization; and Phalloidin conjugated to Alexa Fluor® 568 (A12380, Invitrogen) for F-actin visualization; both apical and basal compartment.

Finally, monolayers were washed two times in PBS, for five minutes; membranes were excised and mounted in glass slides (basal side down), covered with a mixture of Vectashield and PBS (1:3 v:v), a glass cover slip (20x20 mm) sealed with nail polish and stored at 4°C until imaging (within 2-4 days after staining).

Confocal microscopy and image processing

Stained cOEC monolayers were imaged with a laser scanning confocal microscope (Leica SPE-II DMI4000) with diode laser lines of 405 nm, 488 nm and 561 nm at 20x, 40x and 63x magnification and visualized with LAS-AF software. Selection of areas for imaging was based on the following criteria: areas with the most and least secondary cilia; areas with presence of primary cilia; areas with distinct morphological cell characteristics, such as fibroblast presence or cluster formation. Exclusion of outer area of membrane was necessary due to excision interference.

Z-stack acquisition was performed by fixing the 0 z-plane position where F-actin staining was barely visible in the basal surface of the monolayer. The maximum z-plane position was set by switching channels to visualize cilia and moving the z-control to the farthest point of the apical surface, where cilia visualization appeared very dim. Z-step size was set according to the system optimized settings.

Images were further analyzed with Fiji ImageJ software. For each image, a maximum intensity projection, a 3D reconstruction and the orthogonal views were analyzed to determine a representative monolayer score.

Monolayer scoring

The monolayer scoring system was adapted, and further elaborated, from Meeuws (2019), initially based on Chen, et al. (2015).

Representative scores for polarity (presence of primary cilia and columnar shape), overall monolayer presence of secondary cilia, single cell secondary cilia and monolayer confluence were assigned based on the percentage of cells that satisfied each criterion, according to Table 1.

Cell height was measured in Fiji, in a minimum of 30 cells. Average cell height was calculated and a score was assigned.

Table 1. Monolayer scoring criteria.

Score	Polarity (Primary cilia)	Cell differentiation (overall secondary cilia)	Cell differentiation (single cell cilia)	Cell height	Confluence
5	Every cell columnar and with primary cilia	Every cell with secondary cilia (81-100%)	Cell surface completely covered in cilia (81-100%)	≥ 10 μm	Fully confluent (81-100%)
4	Most cells columnar and with primary cilia	Most cells with secondary cilia (61-80%)	Cell surface mostly covered in cilia (61-80%)	5 μm > cell height <10 μm	Mostly confluent (61-80%)
3	Half cells columnar and with primary cilia	Half cells with secondary cilia (41-60%)	Cell surface half covered in cilia (41-60%)	5 μm	Half confluent (41-60%)

2	Few cells columnar and with primary cilia	Few cells with secondary cilia (21-40%)	Cell surface barely covered in cilia (21-40%)	2 μm > cell height <5 μm	Partly confluent (21-40%)
1	Almost no columnar cells with primary cilia	Almost no cells with secondary cilia (6-20%)	Cell surface with less than 5 secondary cilia	2 μm	Few cells on membrane (6-20%)
0	No primary cilia or columnar shape	No cells with secondary cilia (<5%)	No secondary cilia	<2 μm	No cells on membrane (<5%)

Reverse-transcription quantitative PCR

Four different primer pair sequences for JAG1, JAG2, NOTCH1, NOTCH2, NOTCH3, NOTCH4, HES2, HES3, HES4, HES5, HES6, HES7, HEY1, HEY2, HEYL, FOXJ1, RFX1, RFX2 RFX3 and OVGP1 were designed with the NCBI BLAST tool, based on *Canis lupus familiaris* genes. The primer sequences for HES1 were obtained from Dailey, et. al. 2013. Prioritization of genes was done due to the limited RNA concentration in the cOEC monolayer samples. All primer pairs for FOXJ1, RFX1, RFX2, HES1, HES2 and HEY1 were tested on cDNA synthesized from RNA isolated from canine oviductal tissue using the RNeasy Mini Kit (Qiagen) according to the manufacturer's protocol. The selected primer pairs, listed in Table 2, were tested for optimal temperature with a 52°-65° gradient and then standardized using a standard curve.

Epithelial cell monolayers, from two bitches, were released from Matrigel by incubation with Trypsin/EDTA at 38°C for 10 minutes, and pelleted by centrifugation for 5 min at 21°C (300g), followed by RNA isolation with the RNeasy Mini Kit (Qiagen) and cDNA synthesis with random primers and Superscript III (Invitrogen).

RT-qPCR for FOXJ1, RFX1, HES1 and HEY1 was performed in triplicates in 96-well optical reaction plates with SYBR Green interaction dye (BioRad) and quantified by the $\Delta\Delta C_t$ method. Total volume for each reaction was 15 µl containing 7.5 µl SYBR Green mix, 0.075 µl per primer and 1 µl of Rt sample.

Two out of the four selected canine reference genes, presented in Table 3, were successfully standardized (SDHA and B2M) and utilized as endogenous controls for this experiment.

Table 2. Primer sequences for target genes, size of formed products and accession numbers.

Target Gene	Primer Sequence		Product size (bp)	Accession no.
	Forward	Reverse		
FOXJ1	CCATCTACAAGTGGATCACGG	CTTGATGAAGCACTTGTTCAGG	106	XM_005624062.3
RFX1	CCGTTCAGTGGCTCCTAGAC	TGATGCGCAGGCCATAGTAG	222	XM_022406974.1 XM_005632802.3
RFX2	ACAACCATTACCTTCGGCAC	TCTGGTTTCAGACGGATCCC	162	XM_003432794.4
HEY1	ACTTGAGTTCGGCTCTAGGT	ACAAACTGTTATTAATCCGGTCCC	116	NM_001002953.1
HES1	CATCCAAGCCTATCATGGAGA	GTTCCGGAGGTGCTTCACT	161	Dailey et al. 2013
HES2	AGCTTCCCAGTGCTCTCTTG	AGCTTGGGTTGGGTTACCTG	380	XM_005620455.3

Table 3. Reference genes.

Reference Gene	Accession no.	Name	Chromosomal location in *Canis lupus familiaris*
B2M	NM_001284479.1	β-2-Microglobulin	Chromosome 30
GUSB	NM_001003191.1	Glucuronidase-β	Chromosome 6
RPL13	XM_038666767.1	Ribosomal protein L13	Chromosome 5
SDHA	XM_038445573.1	Succinate dehydrogenase complex flavoprotein subunit A	Chromosome 34

Statistics

Data was analyzed with Microsoft Excel and Python. Two-tailed T-student test (significance set at $p < 0.05$) data analysis was performed to compare data sets from different concentrations of DBZ, to compare the control samples to the treated samples and the data sets from each surgery type.

Linear correlations were analyzed with the Pearson correlation coefficient, with significance set at 5% ($\rho < 0.05$).

Analysis of expression fold change was performed in Python.

Results

Oviduct dissection and Canine Oviduct Epithelial Cell (cOEC) isolation

Ovarian bursas from a total of thirty-one bitches were obtained from elective ovariectomy performed either by laparotomy or laparoscopy, from which seven bitches were used for dissection practice and optimization; fifteen bitches, for primary cell culture, DBZ treatment and immunostaining; seven bitches, for RNA extraction for RT-qPCR primer testing and, finally, material from two bitches was discarded due to tissue damage or insufficient material (oviduct pieces shorter than 1.5 cm long).

When compared to dissections at room temperature, dissections performed on ice-mounted petri dishes allowed better management and preservation of the tissue and a prolonged dissection time without any significant changes in the consistency and viscosity of the tissue.

The oviducts of 17 bitches were measured and their length averaged and compared to the weight as shown in Fig 4. Bitches were grouped according to their breed category, in shepherds (3), terriers (2), hounds (2), retrievers (3) and general cross breeds with no visually distinctive traits (7). Grouping bitches by breed type helped portray the

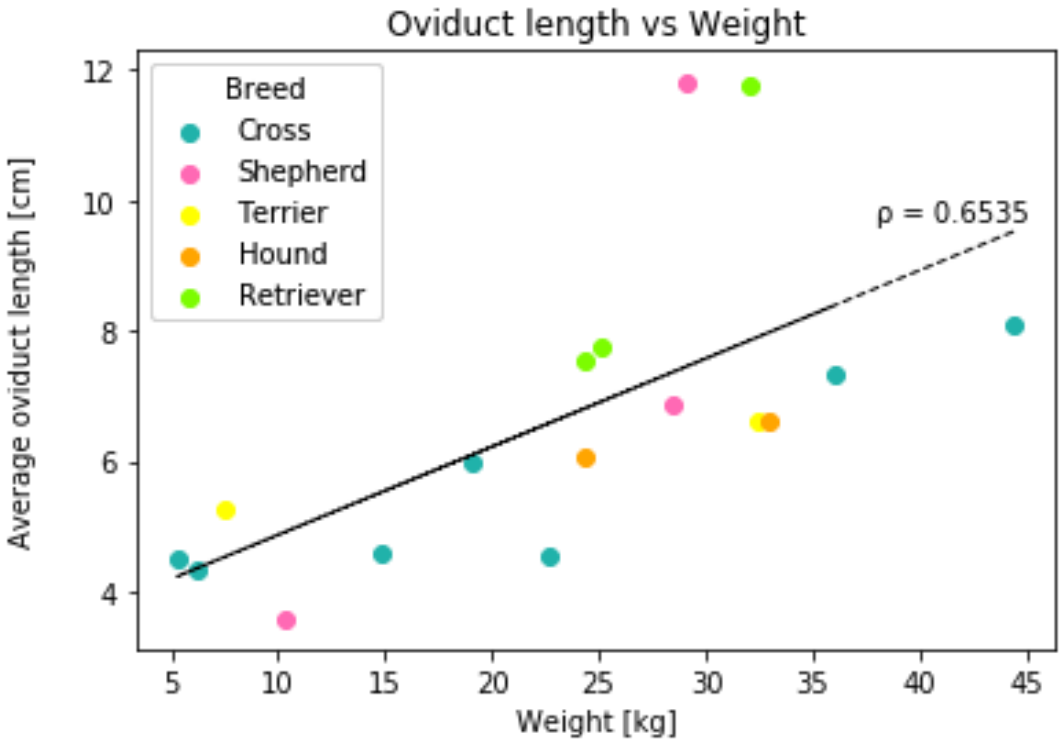

Fig 4. Correlation between the average oviduct length and the weight. Bitches were categorized by breed type to show variability of subjects. Oviduct were measured from end to end, including the infundibulum and UTJ.

wide range and variability of weight and oviduct length within each group. A Pearson coefficient of 0.6535 shows medium-high correlation between the weight of the bitch and the average oviduct length.

Cell yield and viability from the cell extracts were assessed and compared according to each type of ovariectomy (laparoscopy or laparotomy) to determine the optimal surgery type for the obtention of material for our *in vitro* model. Both types of surgery show a low negative Pearson (ρ) correlation between cell yield and viability (Fig 5). Interestingly, a negative correlation indicates that, the bigger the cell count, the less live cells present.

An ANOVA T student test (p = 0.06853) proves no significant difference on the cell yield and viability between each surgery type; consequently, we can determine that cell viability and cell yield do not depend on the type of surgery, if there is no visible or significant tissue damage.

The average cell viability of this study was 44.46% ± 15.41% compared to 40.8% ± 8.8% from Meeuws (2019). These differences may be due to a reduced incubation time with Trypsin-EDTA solution (15 mins Meeuws vs 13 mins this study). A reduced incubation time was utilized in this study to prevent oviduct rupturing during mechanic squeezing and high-density cell clustering in the cell extract prior to culturing. However, the variability was almost twice as high in our study (± 8.8% Meeuws vs ± 15.41% this study); therefore, further experiments need to be carried out in order to improve cell viability, by optimizing digestion time, as well as concentration of Trypsin or by using a different digestion enzyme such as dispase or collagenase.

Meeuws (2019) stained for cytokeratin, proving that this method of enzymatic digestion does indeed retrieve cells from epithelial origin.

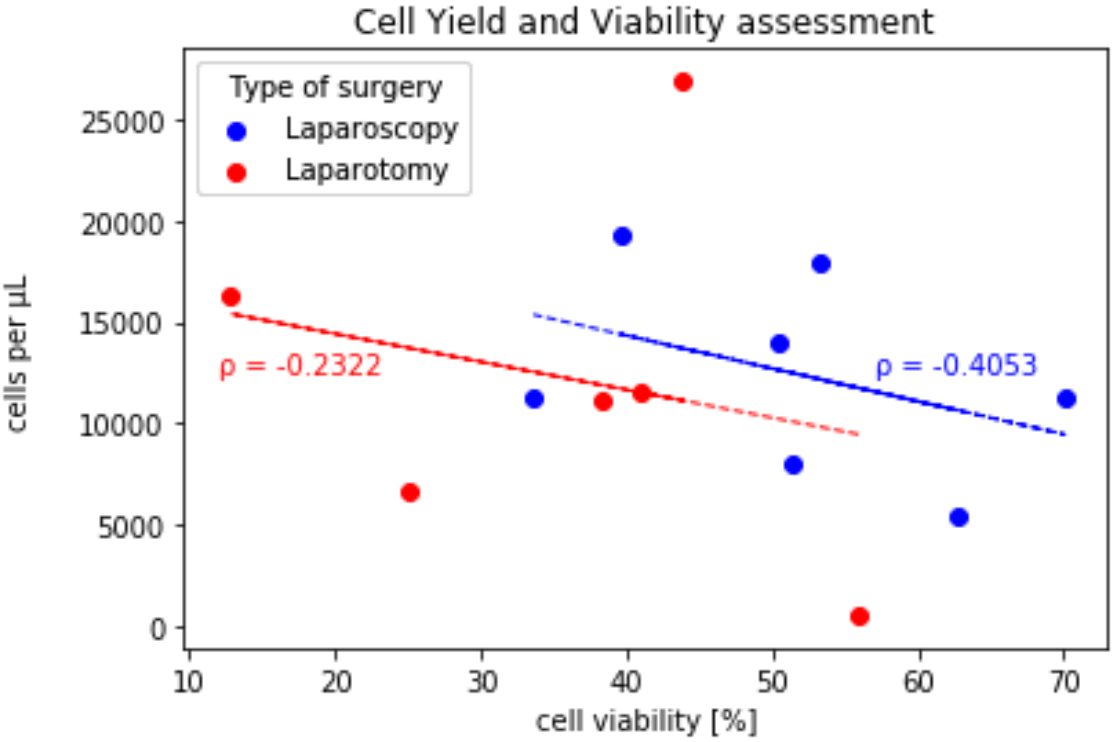

Fig 5. Correlation between cell yield, viability, and type of ovariectomy. Cells from both oviducts were extracted, combined, and assessed for viability and cell yield. Laparoscopic ovariectomies are represented in blue. Ovariectomies by laparotomy are shown in red.

Based on optimal results from previous studies (Thomas, et al. 1995; Meeuws, 2019), the Transwell® membranes in our study were coated with Matrigel. This appeared to promote uniform cell attachment, higher cell density and improved polarization in most of the monolayers, by mimicking the basement membrane of the oviduct lining. However, cell attachment, morphology and polarization were not visible through phase contrast microscopy; therefore, an accurate assessment of the role of the Matrigel coating in improving the monolayer confluence was not possible.

Some monolayers presented, in the center, what appeared to be a stochastic formation of cell clusters in the early stages of culturing in air-liquid interface, as shown in Fig 6.b. Cell clusters varied in size, with the largest presenting visible motile secondary cilia in the perimeter. Individual cells were barely visible (Fig 6.a). Formation of cell clusters was not consistent within different Transwell® inserts from the same sample cultured in the same plates in the exact same conditions (37°C, 5% CO_2). Further studies are required in order to understand what drives cells to cluster together and how this may promote cell differentiation.

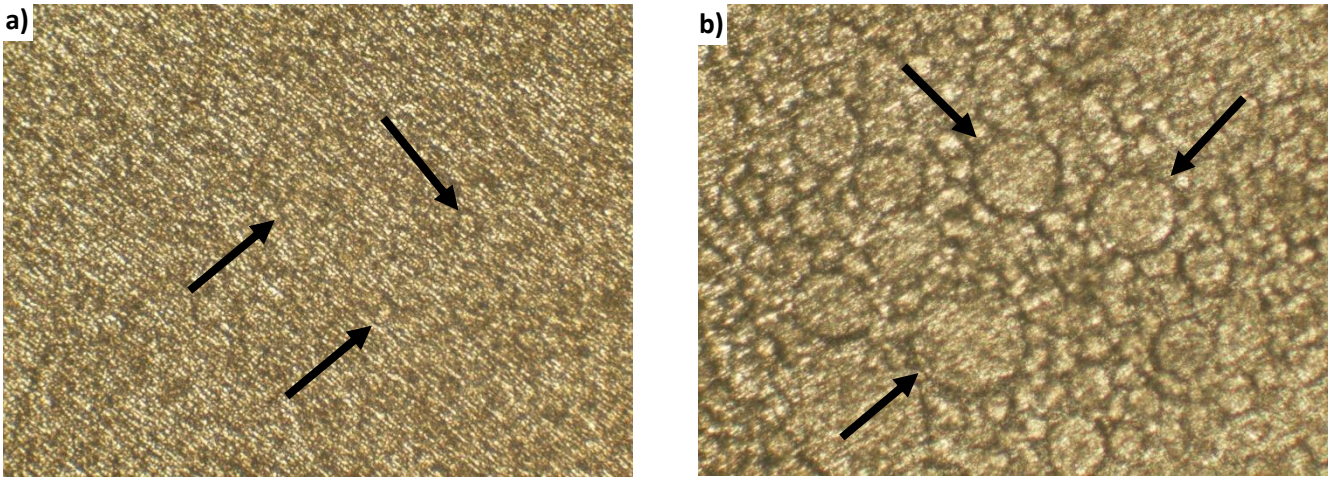

Fig 6. Inverted phase contrast microscopy (20x) visualization of canine epithelial monolayers. a) Single cell visualization is shown by black arrows. Cells appear small and rounded. Sample B08011, insert C2. b) Cell clusters of different sizes formed in some monolayers, which appeared as large round shapes. Motile secondary cilia were possible to visualize in the periphery of most clusters. Sample B14011, insert A2.

Monolayer assessment by immunofluorescent staining

The cOEC monolayers were cultured for 33 days, fixed and immunostained as presented in Fig 7. The nucleus (DAPI) and cytoskeleton (F-actin) staining allowed for a density assessment of the monolayer, as well as individual cell morphology and polarization.

Acetylated α-tubulin was used as a cilia marker. Both primary and secondary cilia were stained and proved to be present only in the apical surface of the Transwell® insert model, serving as evidence of cell polarity. The negative control shows no presence of Alexa Fluor® 488 (green fluorophore).

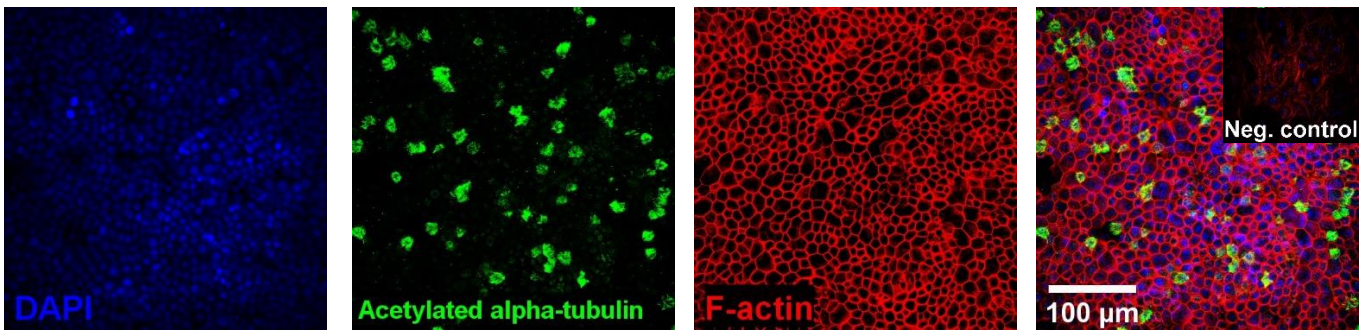

Fig 7. Immunofluorescent staining of cOEC monolayer cultured for 33 days in Transwell® insert (Apical view; 20x magnification). Cells were stained for DAPI, as a DNA (nuclei) marker; acetylated α-tubulin, as a cilia marker and F-actin as a cytoskeleton marker. Sample code B17091_B2. Untreated monolayer (DMSO control)

The effects of the air-liquid interface, in the Transwell® insert model, are shown in Fig 8; where cells from the same bitch (B02091) were seeded in a glass cover slip (Fig 8.a) and a Transwell insert (Fig 8.b) both Matrigel-coated. The cells in the cover slip presented a completely flat and expanded morphology, with expression of acetylated α-tubulin surrounding the nucleus. We attributed the flat morphology and lack of polarity to the weight of the medium on top of the cells in the cover slip. However, presence of fibroblasts in the cover slips or the Transwell® inserts was not

assessed. The Transwell® insert proved to be a better model for promoting cOEC polarization and an increase in cell height and cell density.

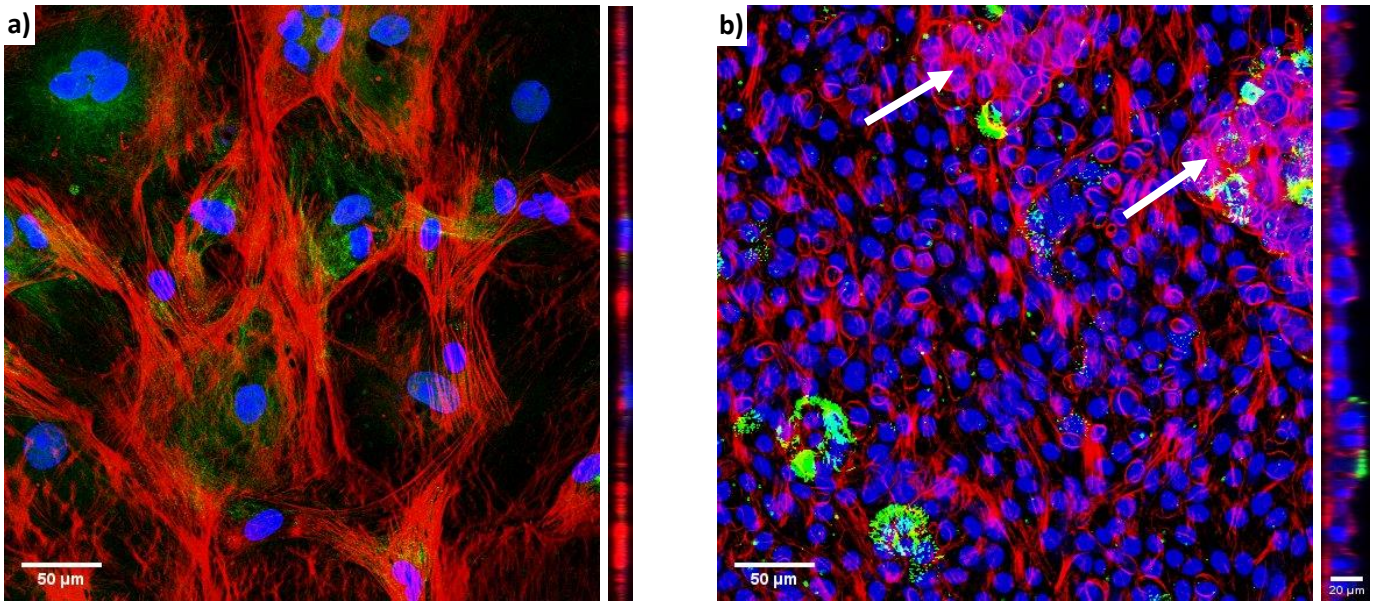

Fig 8. Maximum intensity Z projections and orthogonal views of cOEC monolayers grown for 33 days in glass cover slip vs Transwell insert (Sample B02091; 20x magnification). a) Cells grown in Matrigel-coated glass cover show a flat, expanded morphology and appear to express acetylated α-tubulin around the nuclei. b) Cells seeded in a Matrigel-coated Transwell® insert form a denser monolayer, with mostly columnar cell morphology and some secondary cilia present in the apical surface. Some areas of the monolayer present cell clusters (white arrows) and other areas, closer to the perimeter, present poorer cell polarity and lower cell height (not shown in picture).

We identified two major morphological categories of Transwell® insert cOEC monolayers (Fig 9):

1. Low cell-density monolayers: average count of 27 nuclei per 0.1mm^2
2. High cell-density monolayers: average count of 715 nuclei per 0.1mm^2

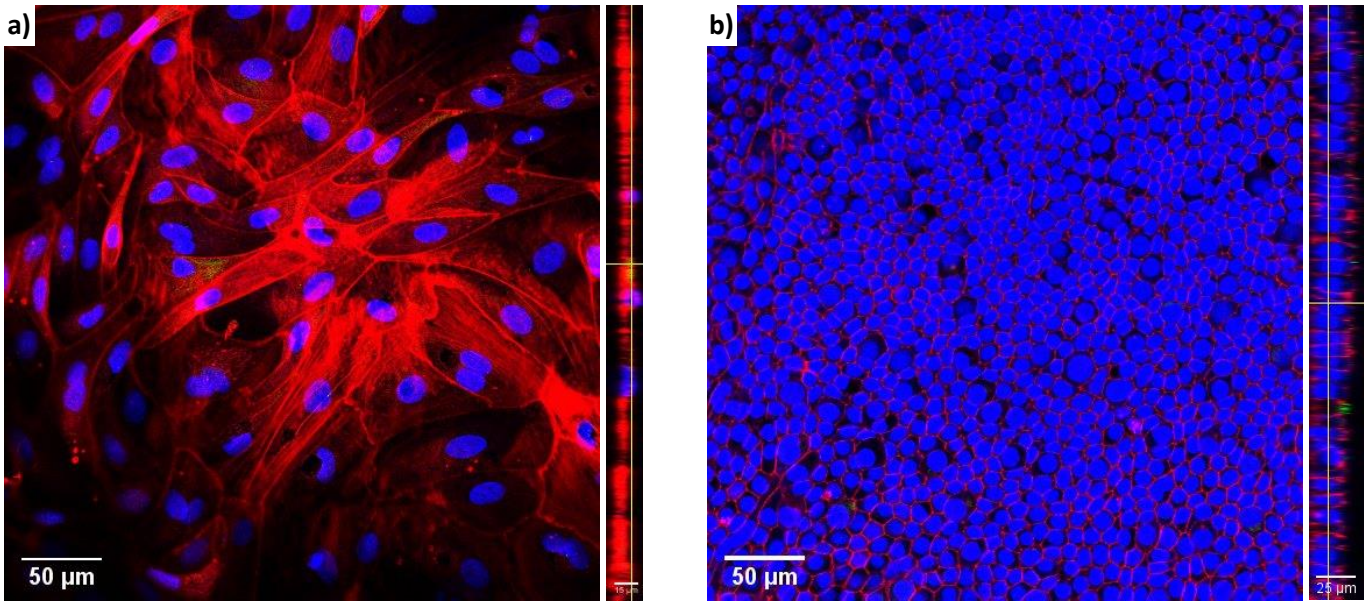

Fig 9. Morphological classification of monolayers based on cell density (20x magnification). Vertical lines in orthogonal views indicate the Z-stack slice shown in frontal view. a) Low cell-density monolayer. (Sample B14092_A1) Flat, expanded cells cover the surface of the Transwell® membrane. Cells have an average height of 15 µm and the nuclei appear to be flat and oval-shaped. b) High cell-density monolayer. (Sample B14091_B2) Cells are columnar, with an average height of 25 µm and densely packed throughout the Transwell® membrane; nuclei appear to be more rounded and spherical.

Low cell-density monolayers

This category of monolayers was mainly characterized by the overall presence of flat cells with expanded, irregular-shaped cytoskeletons. Samples obtained from 3 out of 10 bitches developed a low cell-density monolayer, regardless of the number of viable cells seeded in each insert. There was a lack of cell polarization and, thus, cilia formation (primary or secondary). We identified two types of morphology: elongated and round cells (Fig 10).

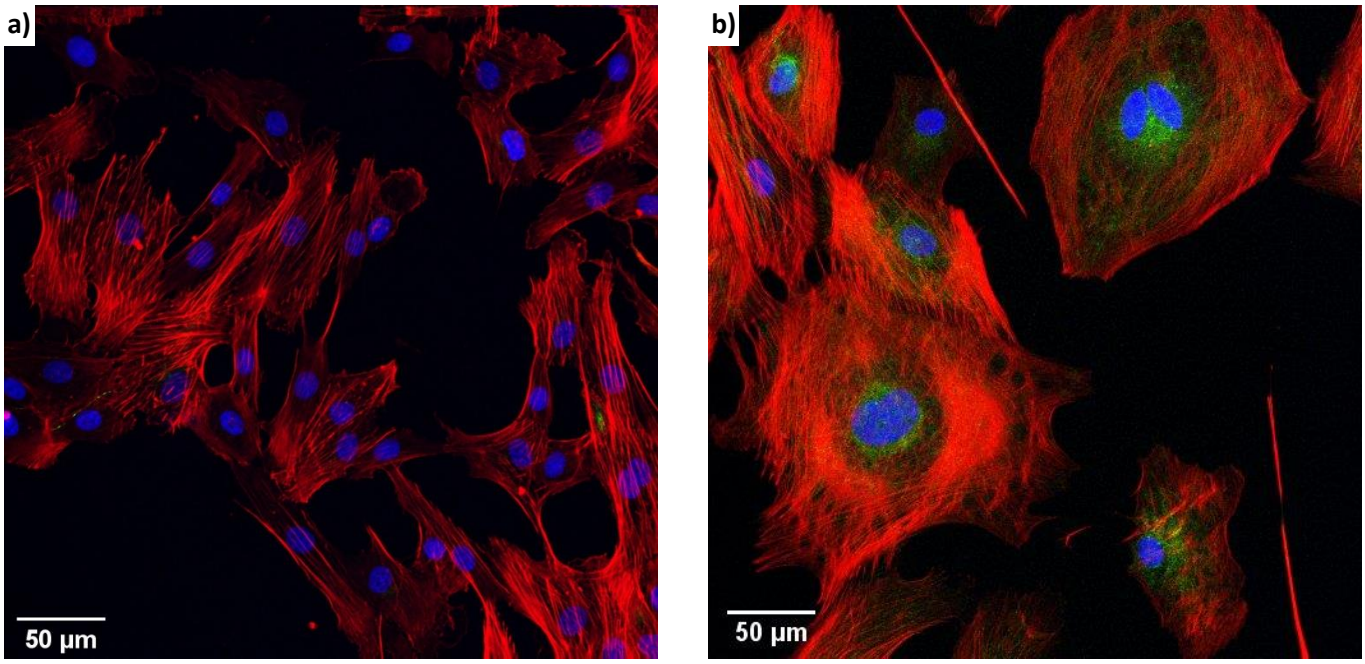

Fig 10. Maximum intensity Z-projections of low-density types of monolayers (20x magnification) a) Elongated morphology. (Sample B28091_C3) b) Round morphology (Sample B08101_B2)

Elongated cells (Fig 10.a) have a fibrous appearance, show irregular cytoskeletal shapes, small nuclei and poor-to-none expression of acetylated α- tubulin; thus,we hypothesize these cells are most likely of fibroblast origin; however, further characterization studies are required to confirm this.

When working with bovine and equine OECs, a pre-culture stage is most frequently performed, where the extracted oviduct cells are seeded in plastic well plates for at least 24 hours, prior to transfering to the Transwell® inserts. This promotes the purification of the cell culture, by allowing the fibroblasts to attach to the preculture wells, since they usually have a faster attachment mechanism than epithelial cells. However, when we performed a preculture stage in the canine sample B10081, we found most cells (>75%) attached to the plate within the first 24 hours, confirming Meeuws (2019) findings about a faster attachment of canine oviduct epithelial cells obtained by enzymatic digestion isolation method. Therefore, we seeded the oviduct extracted cells directly into the Transwell® inserts, increasing the possibilities of fibroblast presence in the monolayers (Appendix 1), but allowing a more direct and fast attachment of the viable epithelial cells into the insert membrane. An optimal preculture phase or other methods of purification of the canine oviduct epithelial cell extract are yet to be described.

Round cells (Fig 10.b) show a more regular, rounded, cytoskeletal shape and large nuclei, surrounded by expression of acetylated α- tubulin. These share most morphological characteristics with the cells grown in glass cover slips (Fig 8.a), therefore we suspect these cells to be of epithelial origin. Additional characterization studies are required to confirm the origin of this cell morpholgy.

High cell-density monolayers

Monolayers with high-cell density shared one single type of cell morphology: densely-packed, polarized, columnar cells (Fig 9.b), with presence of primary and secondary cilia in the apical surface in variable ratios across all samples. This cell morphology resembles the oviduct epithelial lining the most; showing that, for 7 out of 10 bitches, cOEC polarizaton and differentiation was possible to be resumed *in vitro*, even when the cells are retrieved in anestrus.

We observed that monolayers that developed visible cell clusters during the air-liquid interface stage of culturing (days 7 to 22; Fig 6.b) would almost certainly re-differentiate into a polarized, columnar cell shape; with a possible correlation between the amount and size of the cell clusters and the initial overall presence of motile secondary cilia. Supplementary studies are required to confirm this possible correlation.

γ-Secretase inhibition (DBZ) treatment

To assess the effect of the Notch pathway inhibition, by DBZ (10 µM), in the overall presence of ciliated cells, we scored the monolayers according to the following criteria: confluence, polarity and cell differentiation (overall presence of secondary cilia and single cell secondary cilia). The high cell-density monolayers scored higher than low cell-density, since high cell-density monolayers have the desired cell morphology for an optimal oviduct epithelial cell lining model.

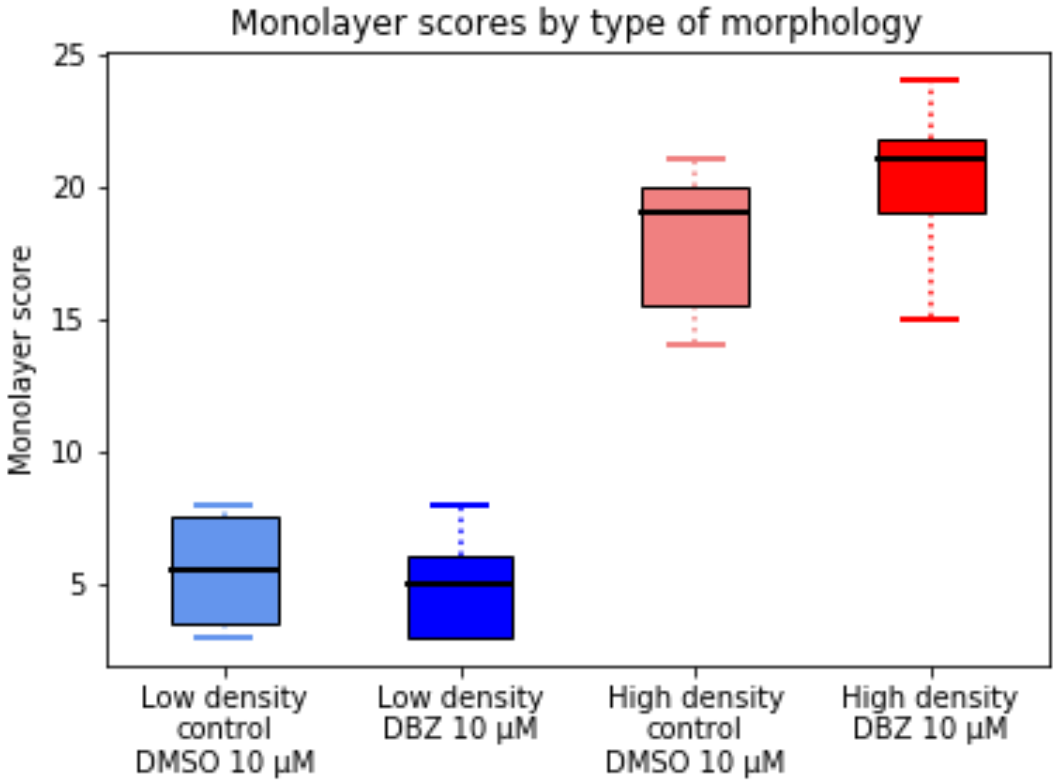

Fig 11. Box plot of monolayer scores by type of morphology. High cell-density monolayers were scored much higher than those with low cell-density.

As presented in Fig 11, there was no statistically-significant difference between scores of monolayers of the same morphological category, treated with DBZ (10 µM) and the control (DMSO) monolayers (high cell-density p=0.075; low cell-density p=0.599). This could be explained by the variability of the presence of secondary cilia, prior to DBZ treatment. In samples where the presence of secondary cilia in the control monolayers was above 15% (samples B31081, B14091, B14011), differentiation toward secondary cilia formation by DBZ treatment had a significant impact, with >70% of cells developing secondary cilia, as presented in Fig 13. However, when secondary cilia presence was below 15% in control monolayers (samples B27081, B02091, B17091), the DBZ treatment had no visible effect. Appendix 2 shows the expression of acetylated α-tubulin in control and DBZ treated high cell-density monolayers and the effect of DBZ in monolayers with diverse ratios of ciliated-to-non-ciliated cells.

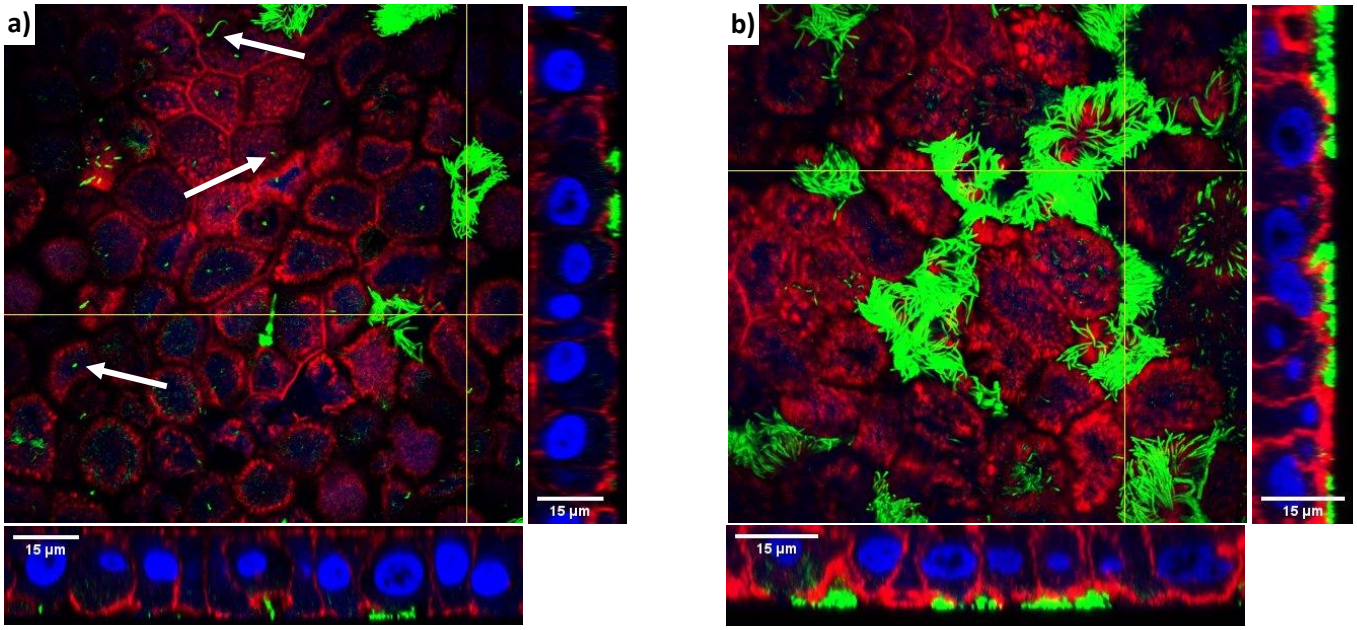

Fig 13. Apical and orthogonal views of cOEC monolayers (Sample B31081 63x magnification). a) DMSO control. Cells in the monolayer present a columnar shape, with height of over 15 µm and primary cilia (white arrows). Few ciliated cells are scattered throughout the monolayer. b) DBZ 10 µM. The monolayer has a high cell density, with good polarization and uniform distribution of bundles of secondary cilia. Cell height is around 15 µm.

Transepithelial electrical resistance (TEER) measurement

We also examined if the DBZ treatment had any effects on the confluence of the monolayers by measuring the relative change in TEER value (Fig 14), with a reference measurement on day 21 (initial TEER value, pre DBZ treatment) and a second measurement on day 32 (final TEER value, post DBZ treatment). We then calculated the relative change in TEER:

$$Relative\ change = \frac{final\ TEER - initial\ TEER}{initial\ TEER}$$

We performed the following two-tailed T-student tests and found no statistically-significant difference in the relative change of TEER values within groups, as described on Table 4:

Table 4. T-student tests for relative change in TEER value.

Two-Sample Test	Scedasticity	p value
Low cell-density control vs high cell-density control	Homoscedastic	0.1527
High cell-density control vs high cell-density DBZ 10 µM	Heteroscedastic	0.1695
Low cell-density control vs low cell-density DBZ 10 µM	Homoscedastic	0.4361
Low cell-density DBZ µM vs high cell-density DBZ 10 µM	Heteroscedastic	0.1695

These results may imply that the relative change in monolayer confluence is most likely independent from the DBZ treatment; thus, Notch inhibition has no effect on the monolayer confluence. However, due to the high variance of

TEER values, we determined that further studies, such as a tracer flux experiment, might be required as a confirmation of these results. (Andriopolou, et al. 1999; Shao, et al. 2010)

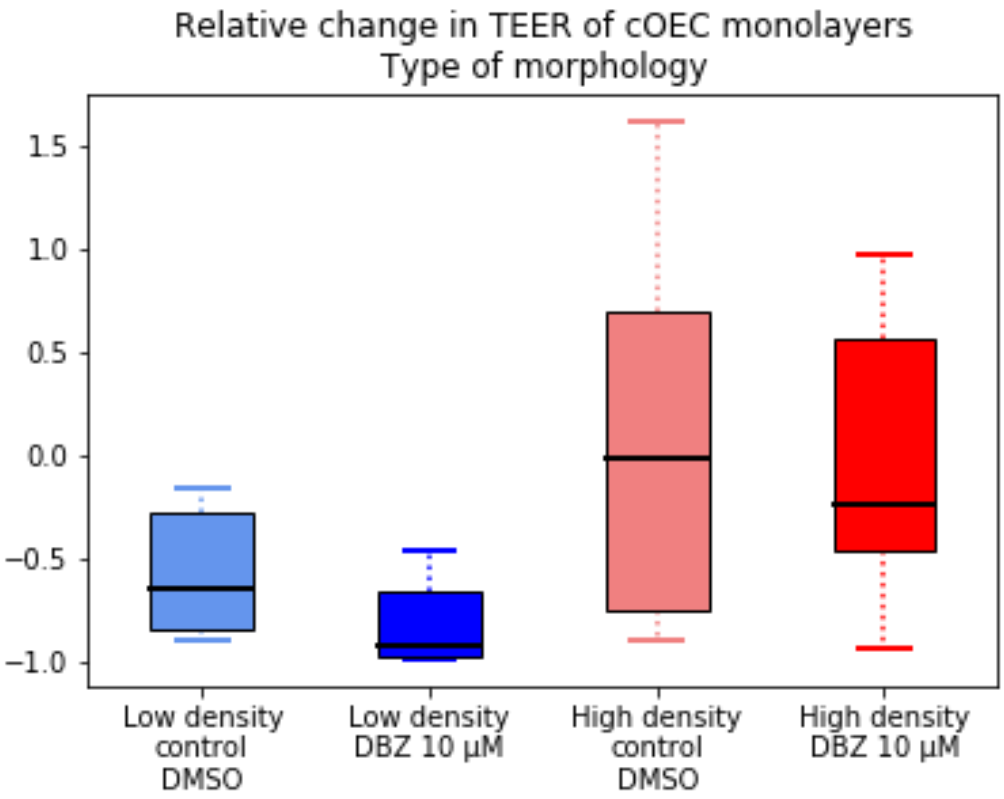

Fig 14. Relative change in TEER by morphological categorization of cOEC monolayers. Outliers for high-density monolayers DBZ 10uM are not shown for visualization purposes, but were indeed considered for the statistical analysis. Outlier values are: 7.14, 20.41, 28.79.

The effect of Notch inhibition in epithelial cell fate and ciliogenesis-related genes

We first compared two material-collection methods for optimal RNA extraction in oviduct tissue. The first collection method was by storing the ovarian bursa in 25 ml PBS and freezing in liquid nitrogen immediately after ovariectomy. The second, was by storing the ovarian bursa in 25 ml of room temperature RNA*later* stabilization solution (Invitrogen), also immediately after ovariectomy. The average concentration of RNA extracted from freezing was 5.65 ng/µL, with an average 260/280 value of 2.23 and a 260/230 value of 0.14. Conversely, the average concentration of RNA extracted from RNA*later* was 124.8 ng/µL, 260/280 value of 2.05 and 260/230 value of 1.28. Thus, we determined that the RNA*later* served as a better collection method for RNA extractions from canine oviduct tissue.

We failed to standardize housekeeping gene RPL13 due to insufficient volume of the primer pairs and GUSB gene due to three different consecutive failed attempts of standard curve experiments at the optimal melting temperature (Appendix 3). We standardized and selected B2M and SDHA as housekeeping genes for the qRT-PCR experiments.

Finally, we evaluated the effect of the DBZ treatment in two samples with high cell-density monolayer morphology: sample B08011 (Fig 15) and sample B14011 (Fig 16), by performing qRT-PCR for ciliogenesis-related transcription factors FOXJ1 and RFX1, and Notch primary target genes HES1 and HEY1. We hypothesized an upregulation in transcription factors FOXJ1 and RFX1 and a downregulation in target genes HES1 and HEY1.

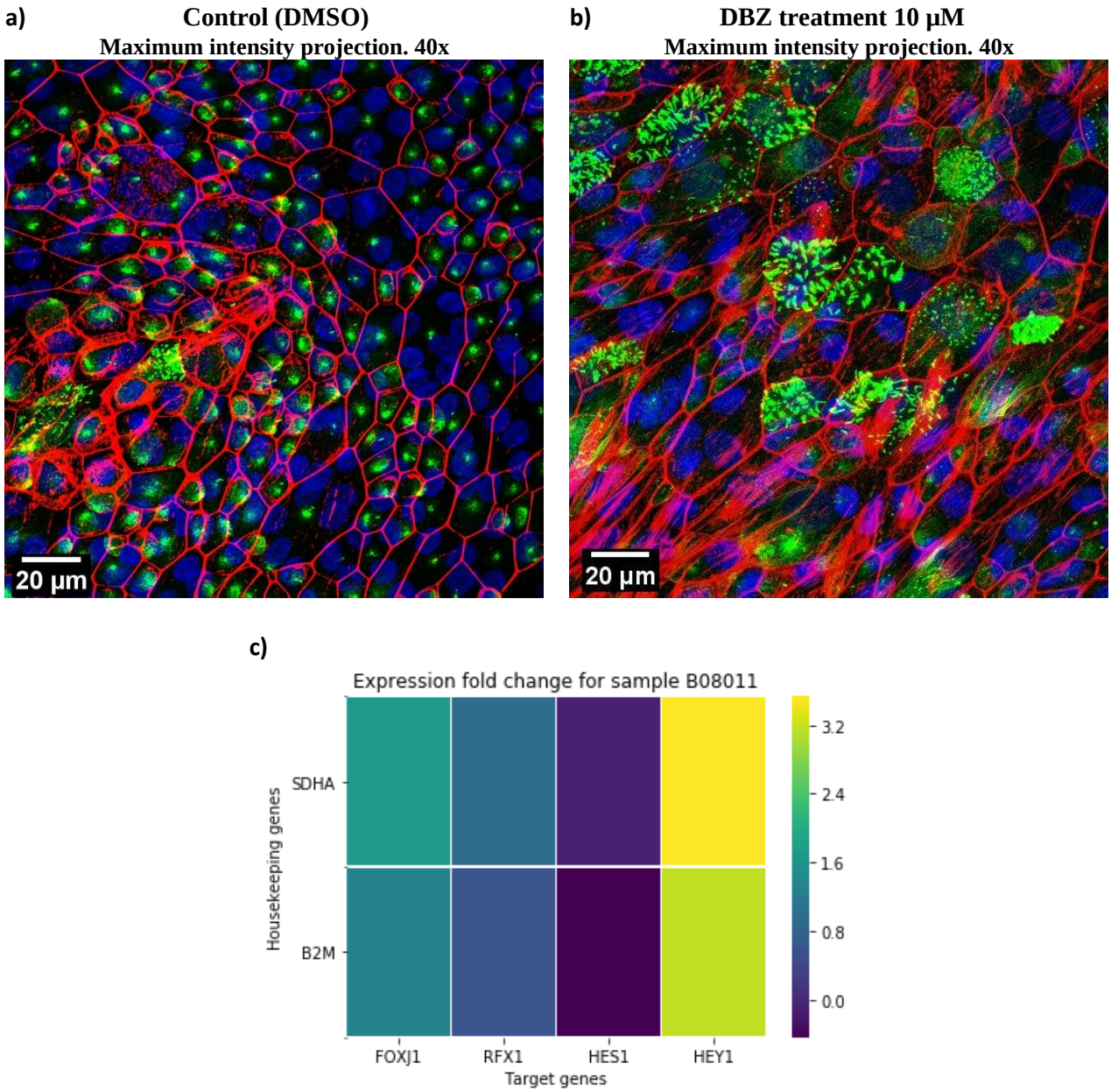

Fig 15. **Effect of Notch inhibition in epithelial cell fate and ciliogenesis-related genes**. **Sample B08011.** Initial cell viability of sample B08011: 50.43%. Number of viable cells per insert: ~422,452 cells. a) Maximum intensity Z projection (40x) of control monolayer (DMSO). Monolayer score 14. b) Maximum intensity Z projection (40x) of DBZ (10 µM) treated monolayer. Score: 21. c) Heat map of expression fold change for FOXJ1, RFX1, HES1, HEY1 genes. Scale bar range -0.5 to 3.5.

Sample B08011 (Fig 15) showed a slight upregulation of the genes FOXJ1 and RFX1; a high upregulation of HEY1 and a slight downregulation of HES1. Results were mostly consistent with our initial hypothesis except for HEY1. The upregulation of HEY1 was unexpected, since it is annotated to be a target gene for Notch, and DBZ inhibits this pathway. Further studies and a larger number of samples are required to understand the upregulation of HEY1.

Sample B14011(Fig 16) showed a slight downregulation of HES1 and HEY1 and slight upregulation of RFX1 and FOXJ1. These results were consistent with our initial hypothesis.

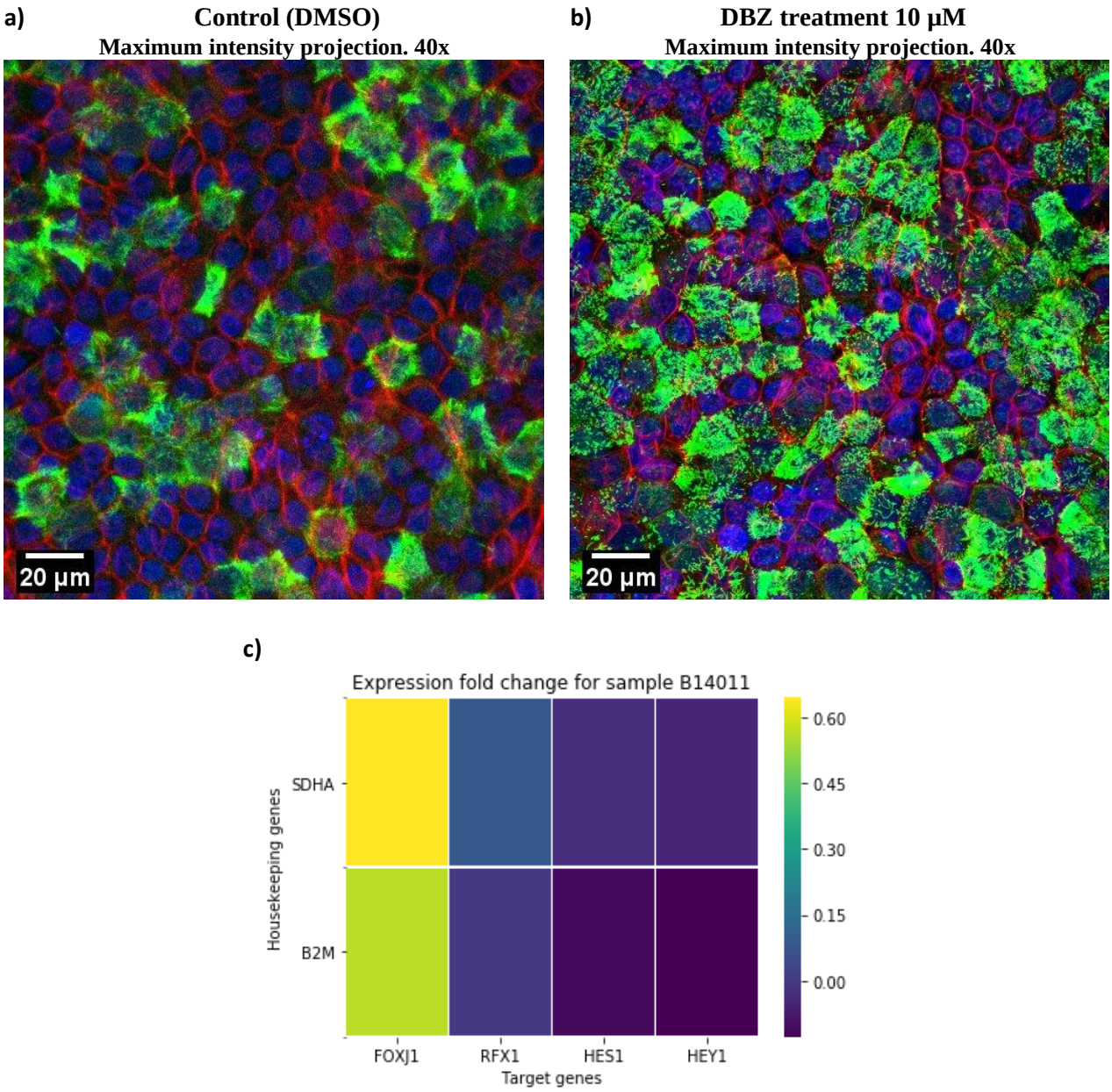

Fig 16. **Effect of Notch inhibition in epithelial cell fate and ciliogenesis-related genes**. **Sample B14011.** Initial cell viability of sample B14011: 33.6%. Number of viable cells per insert: ~227,712 cells. a) Maximum intensity Z projection (40x) of control monolayer (DMSO). Monolayer score 20. b) Maximum intensity Z projection (40x) of DBZ (10 µM) treated monolayer. Score: 24. c) Heat map of expression fold change for FOXJ1, RFX1, HES1, HEY1 genes. Scale bar range -0.10 to 0.65.

Discussion

In the present study, we aimed to optimize the *ex vivo* cOEC isolation and the *in vitro* Transwell® insert model for cOEC monolayer long-term culture. We identified five optimizable major features in the culturing protocol: cell isolation and viability, monolayer morphology, cell polarization, cell re-differentiation and, finally, monolayer hormonal response. In this section, we discuss our approach to optimizing each of these features; and, if necessary, we offer suggestions for possible further optimization.

First, we managed to confirm the ideal time for collection of the ovarian bursas as immediately after ovariectomy. Tissue processing for cOEC isolation must be performed within the first hour after collection, as long as the tissue is kept in refrigeration within this hour.

Cell isolation and viability

We succeeded in improving cell viability after a combination of enzymatic isolation and mechanic squeezing, regardless of the ovariectomy type (laparoscopy of laparotomy), by ~4% when compared to Meeuws' results (2019); this, by working quickly on an ice mounted dissection plate and decreasing the time of incubation with 0.5% Trypsin – 0.2% EDTA solution to 13 min. Dissections performed on ice-mounted petri dishes allowed better management and preservation of the tissue and prolonged dissection time without any significant changes in the consistency and viscosity of the tissue. In addition, reduction in digestion time prevented oviduct rupturing during mechanic squeezing and high-cell density clustering of the cell extract prior to culturing. However, a more significant optimization of cell viability could be achieved by fine tuning the concentration of Trypsin-EDTA solution or utilizing a different digestion enzyme (dispase or collagenase).

Monolayer morphology

We identified two major categories of monolayer morphology, based on cell density. We observed that cells in monolayers with low cell-density shared some morphological features with fibroblasts; however, characterization studies are required to fully confirm the origin of the cells. A vimentin and cytokeratin expression immunofluorescent assay would be a promising approach into further characterizing and confirming the origin of the cells and the fibroblast-to-epithelial cell ratio. Vimentin has been used as a fibroblast marker in multiple studies. (Montoliu, et al. 2006; Aguilera-Rojas, et al. 2020).

As previously mentioned, fibroblast proliferation in the culture might be prevented by the development of a short pre-culture protocol for cOEC. A suggestion would be to more accurately assess attachment times in cOECs, about every 1 to 2 hours after seeding and characterizing the origin of the attached and unattached cells at each time point. Optimal timing of pre-culture will improve the purity in the cOEC culture, as well as compromising less viable cOECs to fast attachment.

Cell polarization

For optimal polarization of high cell-density monolayers, constant monitoring and gently removing any medium leaked into the apical compartment at least once a day, might be necessary. This prevents the weight of the apical medium from applying pressure onto the cell surface and cells not polarizing, as is the case for monolayers grown in a liquid interface in glass cover slips. Less than one third of all our monolayers displayed leaked medium, which usually accumulated in the outer area of the monolayers; however, for some samples the amount of leaked medium was sufficient to cover the whole apical surface. We observed that constantly removing the leaked medium promoted a more uniform height in the columnar cells (for example B31081, Fig 13; B14091, Fig 9b); unlike samples where leaked medium was not removed as often (B02091, Fig. 8b).

The main advantage of the Transwell® insert cOEC monolayer model is, therefore, being able to maintain the air-liquid interface for long-term culture, which allows cells to polarize and maintain a columnar shape, resembling the oviduct epithelial lining *in vivo* morphology. Consequently, we can infer that there is possibly a correlation between the monolayer permeability and cell polarization; however, further studies are required to conform this hypothesis.

Cell re-differentiation

We managed to demonstrate that, for high cell-density monolayers, the air-liquid interface not only allowed cells to polarize into a columnar shape and develop primary cilia, it also promoted cOEC re-differentiation into two major types: ciliated and non-ciliated cells. Ciliated cells were characterized by bundles of secondary cilia present in the apical surface. As previously mentioned, the ratio of ciliated to secretory cells, in vivo, vary among

the estrus stage and the oviductal region, with the highest number of ciliated cells during late follicular and mid-luteal phase in the infundibulum (>60%) and the lowest, during anestrus in the isthmus area (<1%). (Steinhauer, et al. 2004) In this protocol, we aimed for a confluent monolayer model that consistently supports the highest possible ratio of ciliated cells; however, the introduction of an air-liquid interface was not sufficient for promoting the highest ciliated cell ratio. Our approach into further enhancing ciliation, was the inhibition of the Notch pathway by treatment with DBZ. We opted for a 10-day DBZ treatment after 15 days of air-liquid interface, to allow cells to fully polarize before exposure to DBZ.

In our high cell-density control monolayers with a count of ciliated cells of above 15%, the DBZ treatment appeared to have a significant impact, increasing the percentage of ciliated cells to ~80% (Appendix 2). However, this might not be enough evidence to conclude that inhibiting the Notch pathway, by DBZ-induced γ-secretase inhibition, certainly pushes cell re-differentiation towards the formation of secondary cilia. A larger sample size for qRT-PCR experiments is necessary to statistically determine the effects of DBZ in Notch target gene expression and ciliated cell re-differentiation.

Since the effect of the DBZ treatment appeared to be so dependent on the overall initial presence of ciliated cells, and the presence of ciliated cells changes within the estrus cycle (Steinhauer et al. 2004), we hypothesize that by closely monitoring the bitch estrus cycle, and performing the ovariectomy in very early or very late stages of the anestrus period, we might increase the chances of having a higher initial count of ciliated cells, impacting the quality of the Transwell® model, while maintaining the lower risk of complications during surgery. Whether or not ovariectomy time fundamentally plays a role in the re-differentiation of ciliated cells, remains to be determined. Nevertheless, since the estrus cycle varies from bitch to bitch, even within the same species, further studies regarding the optimal ovariectomy time are required.

Some more complex, yet interesting, approaches towards unraveling the mechanisms behind ciliated cell re-differentiation could be gene-editing experiments such as CRISPR-Cas9-based overexpression of the Notch target genes FOXJ1 and RFX1 and silencing expression of Notch receptors or Notch ligands by RNA interference (RNAi).

By measuring the relative change in TEER, we determined that Notch inhibition by DBZ, has no significant effect on the monolayer confluence. These results must be confirmed perhaps by a macromolecular permeability assay, such as an APTS-Dextran Ladder or a paracellular fluorescein tracer flux assays. (Bednarek, 2022)

The effects of DBZ in secretory activity and hormone response of the monolayer have not yet been assessed. Further fundamental research should focus on functionality, secretory activity, and hormone response of the cOEC Transwell® model with and without DBZ-induced enhancement of ciliation. Radioisotopic or fluorescent labelling of estrogen receptors and qRT-PCR of estrogen-dependent genes could perhaps be promising methods to assess the effect of DBZ-based Notch pathway inhibition on hormone response of the monolayer.

In conclusion, in this study we managed to successfully isolate cOECs, from multiple domestic dog breeds, for long-term culture on Matrigel-coated Transwell® inserts, by enzymatic digestion and mechanic squeezing, regardless of the surgery type; with cell viability of 44.46% ± 15.41%. Further optimization of the protocol to improve cell viability is still required.

Cells de-differentiated and formed high- or low-density monolayers in a liquid-liquid interface for the first 7 days of culture, followed by 16 days of culture in an air-liquid interface and, finally, a 10-day 10 μM DBZ treatment. Cells in low density monolayers appeared to share some morphological traits with fibroblasts; however, characterization is required to confirm the origin of these cells. On the other hand, cells in high density monolayers polarized and re-differentiated into columnar epithelial cells, resembling the *in vivo* morphology of the oviduct epithelium, with different ratios of ciliated and non-ciliated cells. The introduction of an air-liquid interface allowed cells to re-differentiate into ciliated and non-ciliated, with a low percentage re-differentiating into ciliated cells. Inhibition of the Notch pathway as a supplementary enhancement of ciliation only had a significant effect in monolayers with an initial ciliated cell ratio of above 15%. Thus, we hypothesized that ovariectomy time (very early or very late stages of anestrus) might play a significant role in the initial percentage of ciliated cells present

in the culture, possibly increasing the chances of a higher percentage of cells re-differentiating into ciliated cells, first by the introduction of an air-liquid interface and then by a DBZ-based inhibition of the Notch pathway.

The sustainability of the culture for long-term, as well as physiological traits and hormone-response of the culture are yet to be studied. An ideal canine oviduct model should be able to support canine IVM, sperm capacitation and IVF. This study serves as a good precedent for future development of the canine oviduct Transwell® model.

References

1 Aguilera-Rojas, M; Sharbati, S; Stein, T; Einspanier, R; (2020) Deregulation of miR-27a may contribute to canine fibroblast activation after coculture with a mast cell tumour cell line, FEBS Open Bio, 10-5, pp. 802-816.

2 Albers-Wolthers, K. Regulation of the hypothalamic-pituitary-gonadal axis in dogs: it starts with a kiss, (2017) Faculty of Veterinary Medicine, Utrecht University, Netherlands, ISBN 978-94-6299-534-5.

3 Andriopoulou, P; Navarro, P; Zanetti, A; Lampugnani, M.G; Dejana, E; (1999) Histamine induces tyrosine phosphorylation of endothelial cell-to-cell adherens junctions. Arterioscler. Thromb. Vasc. Biol. 19, 2286–2297

4 Bednarek, R. (2022). In Vitro Methods for Measuring the Permeability of Cell Monolayers. Methods and Protocols, 5(1), 17.

5 Chastant-Maillard, S; Saint-Dizier, M; Grimard B; Chebrout M; Thoumire S; Reynaud K; (2012) Are oocytes from the anestrous bitch competent for meiosis? Reproduction of domestic animals, 47, pp. 74-79.

6 Chastant-Maillard, S; Chebrout, M; Thoumire S; Saint-Dizier, M; Chodkiewics, M; Reynaud, K; (2010), Embryo biotechnology in the dog: a review, reproduction, fertility and development, 22, pp. 1049-1056.

7 Chen, S; Einspanier, R; Schoen, J; (2013a) Long-term culture of primary porcine oviduct epithelial cells: Validation of a comprehensive in vitro model for reproductive science, Theriogenology, 80, pp. 862-869.

8 Chen, S; Einspanier, R; Schoen, J; (2015) Transepithelial electrical resistance (TEER): a functional parameter to monitor the quality of oviduct epithelial cells cultured on filter supports, Histochemistry and cell biology, 144, pp. 509-515.

9 Choksi, SP; Lauter, G; Swoboda, P; Roy, S; (2014) Switching on cilia: transcriptional networks regulating ciliogenesis. Development. Apr;141(7):1427-41. doi: 10.1242/dev.074666. PMID: 24644260.

10 Coy, P; Garcia-Vázquez, F.A; Visconti, P.E; Avilés, M; (2012) Roles of the oviduct in mammalian fertilization, Reproduction, 144, pp. 649-660.

11 Gier de, J; Kooistra, H.S; Djajadiningrat-Laanen, S.C; Dieleman, S.J; Okkens, A.C; (2006) Temporal relations between plasma concentrations of luteinizing hormone, follicle-stimulating hormone, estradiol-17B, progesterone, prolactin, and a-melanocyte-stimulating hormone during the follicular, ovulatory and early luteal phase in the bitch, Theriogenology, 65, pp.1346-1259.

12 Gualtieri, R; Mollo, V; Braun, S; Barbato, V; Fiorentino, I; Talevi; (2013) Bovine oviductal monolayers cultured under three-dimension conditions secrete factors able to release spermatozoa adhering to the tubal reservoir in vitro, Theriogenology, 79, pp. 429-435.

13 Halter, S; Reynaud, K; Tahir, Z; Chastant-Maillard, S; Saint-Dizier, M; (2011) The mammalian oviduct revisited, Gynécologie Obstétrique & Fertilité, 39, pp. 625-629.

14 Hu, M; Du, Z; Zhou, Z; Long. H; Ni, Q; (2020) Effects of serum and follicular fluid on the in vitro maturation of canine oocytes, Theriogenology, Volume 143, Pages 10-17, ISSN 0093-691X.

15 Jingu No, Minghui Zhao, Seunghoon Lee, Sun A. Ock, Yoonseok Nam, Tai-Young Hur, (2018) Enhanced in vitro maturation of canine oocytes by oviduct epithelial cell co-culture, Theriogenology, Volume 105, Pages 66-74, ISSN 0093-691X.

16 Lawrenson, K; Notaridou, M; Lee, N; Benjamin, E; Jacobs, I.J, Jones, C; Gayther, S.A; (2013) In vitro three-dimensional modeling of fallopian tube secretory epithelial cells, BMC Cell Biology, 14, pp. 1-15.

17 Lee, S.H; Oh, H.J; Kim M.J; Kim. G.A; Choi. Y.B; Jo, Y.K; Setyawan, R.M.N; Lee, B.C; (2017) Oocyte maturation-related gene expression in the canine oviduct, cumulus cells, and oocytes and effect of co-culture with oviduct cells on in vitro maturation of oocytes, Journal of assisted reproduction and genetics, 34, pp. 929-938.
18 Lee, W.M; Kooistra, H.S; Mol, J.A; Dieleman, S.J; Schaefers-Okkens, A.C; (2006) Ovariectomy during the luteal phase influences secretions of prolactin, growth hormone, and insulin-like growth factor-I in the bitch, Theriogenology, 66, pp. 484-490.
19 Leemans, B., Bromfield, E. G., Stout, T. A., Vos, M., Van Der Ham, H., Van Beek, R., ... & Henning, H. (2022). Developing a reproducible protocol for culturing functional confluent monolayers of differentiated equine oviduct epithelial cells (dagger). Biology of reproduction.
20 Montoliu, P; Añor, S; Vidal, E; Pumarola, M; (2006) Histological and Immunohistochemical Study of 30 Cases of Canine Meningioma, Journal of Comparative Pathology, Volume 135-4, pp 200-207.
21 Murta, D; Batista M; Trindade A; Silva E; Mateus L; Duarte A; Lopes-da-Costa L. (2015) Dynamics of Notch signalling in the mouse oviduct and uterus during the oestrous cycle. Reproduction, Fertility and Development 28, pp. 1663-1678.
22 Nagashima, J.B; Sylvester, S.R; Nelson, J.L; Hon Cheong, S; Mukai, C; Lambo. C; Flanders. J.A; Meyers-Wallen, V.N; Songsasen, N; Travis, A.J; (2015) Live births from domestic dog (Canis familiaris) embryos produces by in vitro fertilization, PLOS ONE, 10 (12), pp. 1-13.
23 No, J; Zhao, M; Lee, S; Ock; S.A; Nam, Y; Hur, T.Y; (2018) Enhanced in vitro maturation of canine oocytes by oviduct epithelial cell co-culture, Theriogenology, 105, pp. 66-74.
24 Purvis, T. L; Hearn, T; Spalluto, C; Knorz, V. J; Hanley, K. P; Sanchez-Elsner, T; Hanley, N. A. and Wilson, D. I. (2010). Transcriptional regulation of the Alström syndrome gene ALMS1 by members of the RFX family and Sp1. Gene 460, pp. 20-29.
25 Senger, P.L; (2012) Pathways to pregnancy & parturition, 3rd edition, pp. 26-30.
26 Shao, J; Wu, L; Wu, J. et al. (2010) A microfluidic chip for permeability assays of endothelial monolayer. Biomed Microdevices 12, pp. 81–88.
27 Sostaric, E; S. J. Dieleman, C. H. A. van de Lest, B. Colenbrander, P. L. A. M. Vos, N. Garcia-Gil, and B. M. Gadella. (2008) Sperm binding properties and secretory activity of the bovine oviduct immediately before and after ovulation. Mol. Reprod. Dev. 75:60–74.
28 Steinhauer, N; Boos, A; Günzel-Apel, A.R; (2004) Morphological changes and proliferative activity in the oviductal epithelium during hormonally defined stages of the oestrous cycle in the bitch, Reproduction in domestic animals, 39, pp. 110-119.
29 Thomas, P.G.A; Ignotz, G.G; Ball, B.A; Miller, P.G; Brinkso, S.P; Currie, B; (1995) Isolation, culture and characterization of equine epithelial cells in vitro, Molecular reproduction and development, 41, pp. 468-478.
30 Tsao, P-N; Vascolncelos, M. Izvolsky, K; Qian, J; Lu, J. and Cardoso, W. V. (2009) Notch signaling controls the balance of ciliated and secretory cell fates in developing airways. Development and Disease, 136, 2297-2307.
31 Ulbrich, S. E; K. Zitta, S. Hiendleder, and E. Wolf. (2010) In vitro systems for intercepting early embryo-maternal cross-talk in the bovine oviduct. Theriogenology, 73:802– 816.
32 Yu, X; Ng, C; Habacher, H. et al. (2008) Foxj1 transcription factors are master regulators of the motile ciliogenic program, Nat Genet 40, 1445–1453. https://doi.org/10.1038/ng.263.
33 Zhu, M; Iwano, T. and Takeda, S; (2019) Estrogen and EGFR Pathways Regulate Notch Signaling in Opposing Directions for Multi-Ciliogenesis in the Fallopian Tube. Cells, 8, 93.

Appendix 1. Sample B17091 insert A3 (DMSO control 10 µM).

The monolayer in insert A3 of the sample B17091 presented some areas with a) low density of cells (flat, expanded, very few primary cilia) and other areas with b) high density of cells (columnar morphology with an average cell height of 22 µm. Polarized cells with few primary cilia but no secondary cilia). This raises further possibilities that the oviduct cell extract might contain a mix culture of epithelial cells with fibroblast. Nonetheless, further studies are needed to evaluate the origin of the cells and an optimal method for purification of epithelial cells.

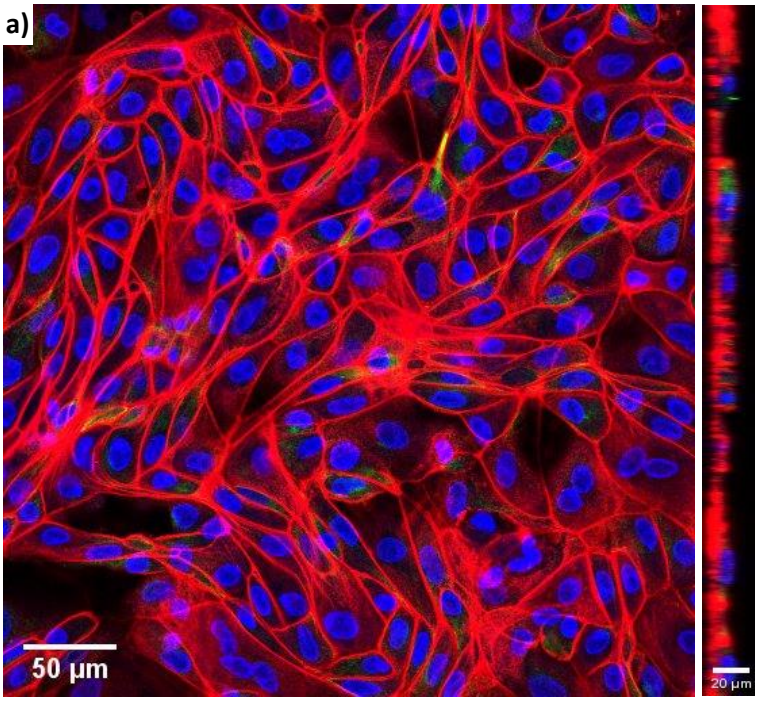

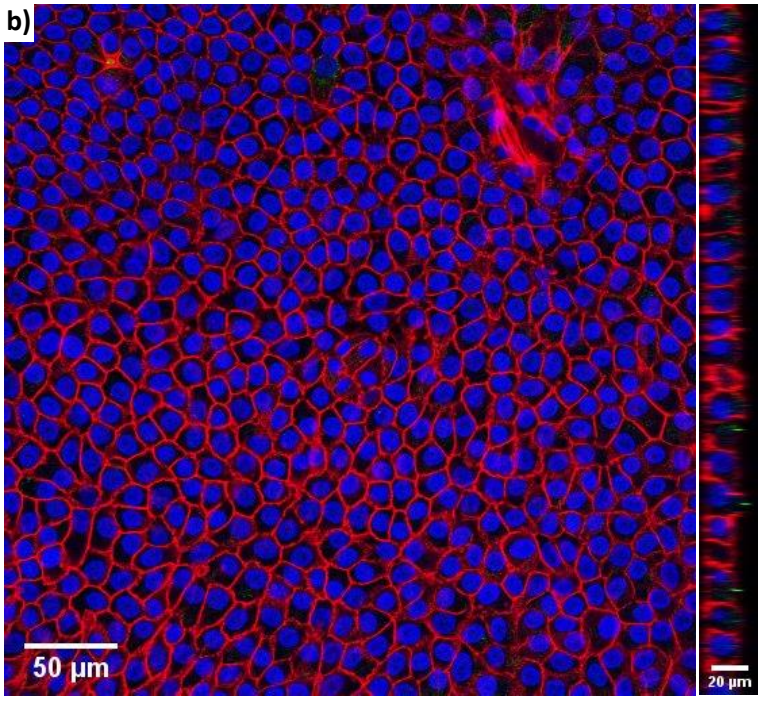

Appendix 2. Maximum intensity Z projections of expression of acetylated α-tubulin in high cell-density monolayers with different ratios of ciliated cells.

a) Sample B17091_B2 (DMSO control). Few cells with secondary cilia are scattered only in the central area of the monolayer (<15%)
b) Sample B17091_B1 (DBZ 10 µM). The treatment appeared to have no effect in promoting formation of secondary cilia.
c) Sample B14091_C1 (DMSO control). Few cells with secondary cilia are scattered all over the monolayer (~20%)
d) Sample B14091_A1 (DBZ 10 µM). The treatment highly promoted the formation of secondary cilia across the monolayer (~80%)
e) Sample B14011_D2 (DMSO control). About half of the cells in the monolayer are ciliated (40 – 60%)
f) Sample B14011_D1 (DBZ 10 µM). The treatment highly promoted the formation of secondary cilia across the monolayer (~80%)

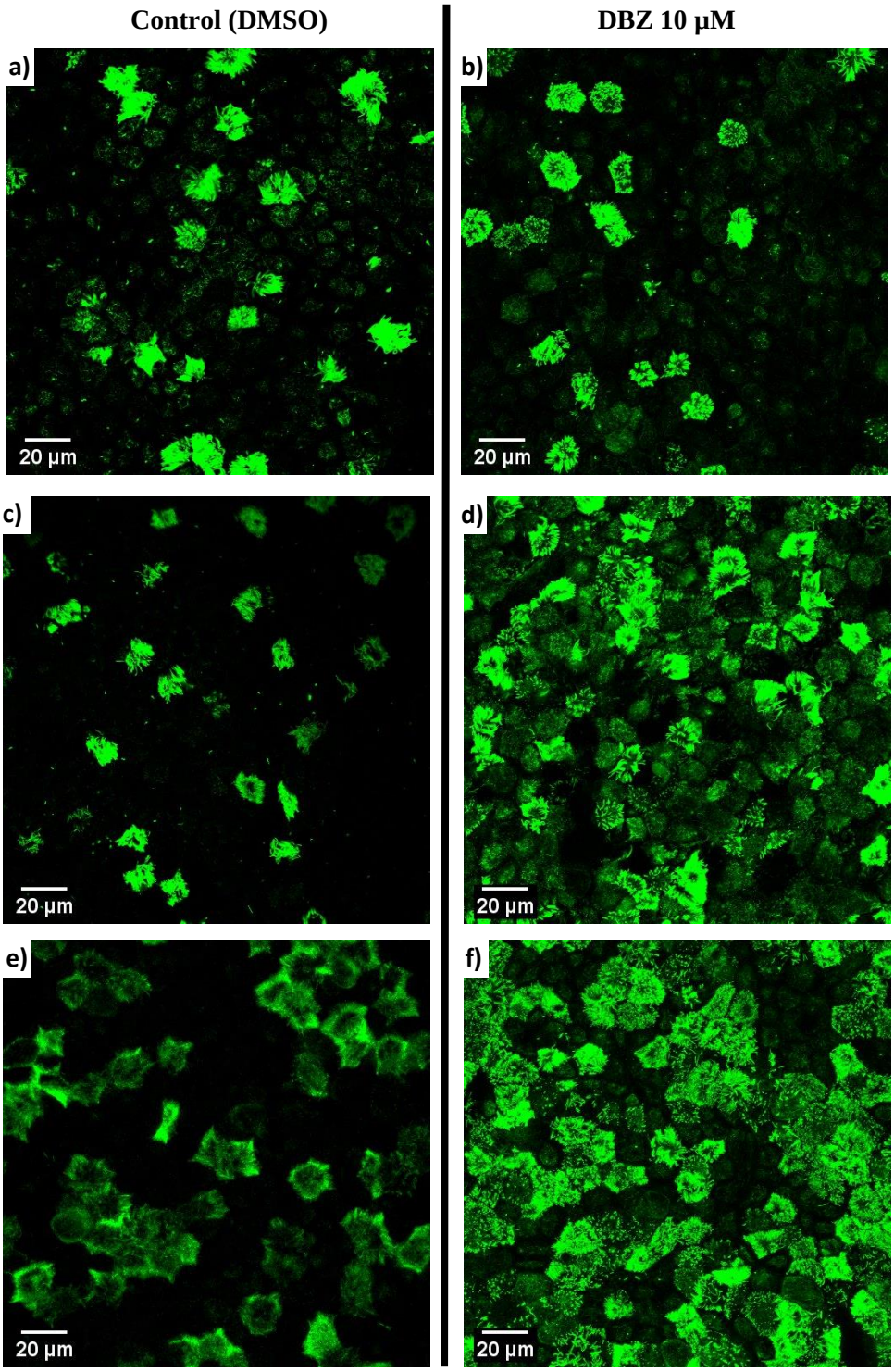

Appendix 3. GUSB primer failed standard curves.